



HAL
open science

Tungsten (VI) speciation in hydrothermal solutions up to 400°C as revealed by in-situ spectroscopy

Eleonora Carocci, Laurent Truche, Michel Cathelineau, Marie-Camille Caumon, Elena F. Bazarkina

► To cite this version:

Eleonora Carocci, Laurent Truche, Michel Cathelineau, Marie-Camille Caumon, Elena F. Bazarkina. Tungsten (VI) speciation in hydrothermal solutions up to 400°C as revealed by in-situ spectroscopy. *Geochimica et Cosmochimica Acta*, 2021, 317, pp.306-324. 10.1016/j.gca.2021.11.004 . hal-03431203

HAL Id: hal-03431203

<https://hal.univ-lorraine.fr/hal-03431203v1>

Submitted on 16 Nov 2021

HAL is a multi-disciplinary open access archive for the deposit and dissemination of scientific research documents, whether they are published or not. The documents may come from teaching and research institutions in France or abroad, or from public or private research centers.

L'archive ouverte pluridisciplinaire **HAL**, est destinée au dépôt et à la diffusion de documents scientifiques de niveau recherche, publiés ou non, émanant des établissements d'enseignement et de recherche français ou étrangers, des laboratoires publics ou privés.



Distributed under a Creative Commons Attribution - NonCommercial - NoDerivatives 4.0 International License

1 **TUNGSTEN (VI) SPECIATION IN HYDROTHERMAL SOLUTIONS UP TO**
2 **400°C AS REVEALED BY IN-SITU RAMAN SPECTROSCOPY**

3 Eleonora Carocci ^{a, b*}, Laurent Truche ^c, Michel Cathelineau ^a, Marie-Camille Caumon^a, and Elena
4 F. Bazarkina ^{d, e, f, g}

5
6 ^a *Univ. Lorraine, GeoResources, CNRS, 54000, Nancy, France*

7 ^b *Department of Earth and Environmental Sciences, Ludwig-Maximilians-Universität,*
8 *Theresienstraße 41, München 80333, Germany*

9 ^c *Univ. Grenoble Alpes, CNRS, ISTERRE, F-38041 Grenoble, France*

10 ^d *Univ. Grenoble Alpes, CNRS, INSTITUT NÉEL, 25 Avenue des Martyrs, F-38042 Grenoble Cedex*
11 *9, France*

12 ^e *Institute of Geology of Ore Deposits, Petrography, Mineralogy and Geochemistry, Russian*
13 *Academy of Sciences (IGEM RAS), 35 Staromonetny per., Moscow 119017, Russia*

14 ^f *The Rossendorf Beamline at ESRF, The European Synchrotron, CS40220, 38043 Grenoble*
15 *Cedex 9, France*

16 ^g *Institute of Resource Ecology, Helmholtz Zentrum Dresden-Rossendorf (HZDR), PO Box 510119,*
17 *01314 Dresden, Germany*

18

19 * Email: eleonora.carocci@min.uni-muenchen.de

20

21 **Keywords:**

22 Tungsten polymers; Polytungstates, Fused silica glass capillary technique; Ore deposits

23

24

25

26

27

28

29

30 Abstract

31 Tungsten (VI) speciation in hydrothermal solutions is investigated through in-situ Raman spectroscopy coupled with the
32 fused silica glass capillary technique at temperatures up to 400 °C. The effect of temperature, pH, chlorinity and carbonate
33 speciation are evaluated. At all investigated temperatures, the tungstate ion WO_4^{2-} (927 cm^{-1}) is the only W species in
34 solution at $\text{pH} > 10$. At a given pH, the presence of dissolved carbonates and chloride does not affect the tungsten
35 speciation. Tungsten polymers remain stable up to 400 °C under acidic to circum-neutral pH conditions and total tungsten
36 concentration above $0.01\text{ mol}\cdot\text{kg}_{\text{H}_2\text{O}}^{-1}$. Among the three observed polymers, namely $[\text{W}_7\text{O}_{24}]^{6-}$ (paratungstate-A, ~ 960
37 cm^{-1}), $[\text{W}_{10}\text{O}_{32}]^{4-}$ (tungstate-Y, $\sim 970\text{ cm}^{-1}$), and $\alpha\text{-}[\text{H}_2\text{W}_{12}\text{O}_{40}]^{6-}$ (α -metatungstate, $\sim 990\text{ cm}^{-1}$), only the hepta- and
38 dodeca-tungstate are stable at elevated temperature. Combined with revised literature data, these results allow the
39 thermodynamic stability constants of these W polymers to be constrained, enabling quantitative predictions of their
40 relative abundance at temperatures up to 300 °C. These predictions suggest that W polymerization occurs under
41 hydrothermal conditions even at low W concentration (down to $10^{-5}\text{ mol}\cdot\text{kg}_{\text{H}_2\text{O}}^{-1}$) under acidic conditions. These
42 observations imply that the currently available geochemical models on W transport and deposition in deep and hot
43 geological fluids need to be revised.

44

45 1. Introduction

46 The knowledge of tungsten (W) speciation in hydrothermal solutions is of primary importance to develop
47 geochemical models for tungsten ore deposits genesis. W mobility in deep and hot geological fluids is currently poorly
48 constrained despite a consensus that W is predominantly transported in the ore-forming fluids as W(VI) anions with
49 negligible chloride complexation. The few rare models of hydrothermal transport and deposition of tungsten are based on
50 tungsten speciation dominated by tungstic acid (H_2WO_4^0) and its dissociation products HWO_4^- and WO_4^{2-} (Heinrich,
51 1990; Gibert et al., 1992, Wood and Samson, 2000). This relatively simple aqueous W speciation model at elevated
52 temperature (T) and pressure (P) mainly relies on the interpretation of data on W-bearing minerals solubility from quench
53 experiments available at that time (Eugster and Wilson, 1985; Wood and Vlassopoulos, 1989; Wood, 1992). Wang et al.
54 (2019) recently investigated W solubility and speciation in NaCl-bearing solutions up to 350 °C through quenched
55 solution analysis. They demonstrated that NaCl concentration does not affect the solubility of tungsten trioxide. They
56 also concurred with a W speciation dominated by monomeric tungstate species over the entire pH range at T up to 350
57 °C.

58 This view of W speciation under hydrothermal condition contrasts with the already well-studied W speciation at ambient
59 T-P, where the coexistence of several polyanions containing 6, 7, 10, and even 12 W-atoms depending on pH is
60 demonstrated (Duncan and Kepert, 1961; Aveston, 1964; Arnek and Sasaki, 1974; Häufe, 1982; Ng and Gulari, 1984;
61 Cruywagen and Van Der Merwe, 1987; Gumerova and Rompel, 2020). It also ignores or simplifies the conclusions of
62 two pioneering studies reporting in-situ measurements of W speciation under hydrothermal conditions. First, Wesolowski
63 et al. (1984) provided the results of potentiometric titrations of tungstate-bearing solution in the range 100-300 °C and
64 revealed that polytungstates ($\text{H}_{10}(\text{WO}_4)_6^{2-}$, $\text{H}_7(\text{WO}_4)_6^{5-}$, $\text{H}_{18}(\text{WO}_4)_{12}^{6-}$) dominate the speciation in the $10^{-2}\text{ mol}\cdot\text{kg}_{\text{H}_2\text{O}}^{-1}$
65 solution below pH 5. This later total W concentration (i.e. about 2000 ppm) is already relatively high compared to natural
66 ore-forming fluids. However, it is not irrelevant as W concentrations $> 1000\text{ ppm}$ are frequently reported from in-situ

67 analysis of fluid inclusions associated with W-ore deposits (Korges et al., 2018; Beuchat et al., 2004). At lower W
68 concentrations, the monomers (HWO_4^- and WO_4^{2-}) become increasingly stable, but at least one polymer ($\text{H}_{10}(\text{WO}_4)_6^{2-}$)
69 remains predominant at pH below 3 up to 350 °C. Second, thanks to in-situ Raman spectroscopy, Bilal et al. (1986)
70 showed two stable polymeric W-species, $\text{W}_{10}\text{O}_{32}^{4-}$ and $\text{H}_3\text{W}_{12}\text{O}_{40}^{5-}$, that dominate the W speciation at T up to 200 °C
71 under acidic and circum-neutral conditions (W concentration in their experiments was not provided but it is supposedly
72 $\geq 0.01 \text{ mol.kg}_{\text{H}_2\text{O}}^{-1}$). They did not succeed in detecting the presence of HWO_4^- over the 3-9 pH range and concluded that
73 the polymerization degree increases with increasing temperature and pressure. Recently, Wang et al. (2020a, 2020b)
74 performed an in-situ Raman spectroscopic investigation of the hydrothermal speciation of tungsten under moderately
75 acidic (pH > 4 at room T) to alkaline conditions and W concentrations down to $0.005 \text{ mol.kg}_{\text{H}_2\text{O}}^{-1}$. Although these authors
76 unambiguously detected the presence of polymeric species of W under somewhat acidic conditions, at least at T up to
77 300 °C, they ignored them in their thermodynamic modelling. Interestingly, as mentioned above, the W polymers
78 supposed to be present at elevated temperature do not correspond to those well identified at ambient conditions such as
79 paratungstate A ($\text{W}_7\text{O}_{24}^{6-}$, with a C_{2v} symmetry), paratungstate B ($\text{H}_2\text{W}_{12}\text{O}_{42}^{10-}$, with a C_1 symmetry) or α -metatungstate
80 ($\text{H}_2\text{W}_{12}\text{O}_{40}^{6-}$, with a Keggin structure). To our knowledge, these four studies (Wesolowski et al., 1984; Bilal et al., 1986;
81 Wang et al., 2020a, 2020b) are the only ones that document W speciation under hydrothermal conditions using in-situ
82 techniques. They demonstrate that polymeric W-species may remain in solution at elevated T-P and circumneutral to
83 acidic pH conditions and display significant disagreements regarding the polymer nature and their respective stability.

84 To fill this gap, we used quantitative in-situ Raman spectroscopy on W-bearing aqueous solutions at T up to 400
85 °C to determine the identity, stability, concentrations and thermodynamic properties of dissolved tungsten species in the
86 Na-WO₄-Cl-CO₂-H₂O system over a wide range of pH and tungstate/chloride concentrations. This new data allows for
87 the first-time quantitative predictions of the abundance of W polymers in geological fluids and the evaluation of their role
88 on W transport and deposition in ore deposits.

89 2. Methods

90 2.1. Experiments

91 Tungsten salts - sodium tungstate dihydrate ($\text{Na}_2\text{WO}_4 \cdot 2\text{H}_2\text{O}$, @Sigma-Aldrich) or sodium metatungstate hydrate
92 ($\text{Na}_6\text{W}_{12}\text{O}_{39}\text{H}_2\text{O}$, @Sigma-Aldrich) - were dissolved in milli-Q water (resistivity of $18.2 \text{ M}\Omega\text{-cm}$ at 25 °C) to prepare the
93 W-bearing aqueous solution. The initial total W concentration was generally set to 0.1 m ($\text{mol.kg}_{\text{H}_2\text{O}}^{-1}$), but some
94 experiments were conducted at lower W concentrations (0.01 and 0.05 m). The effect of pH, chlorinity and dissolved
95 carbonate/bicarbonate concentration on W speciation was studied by mixing a known amount of the following reagents:
96 NaCl, NaOH, HCl, HCOOH, CH₃COOH, NH₄Cl, CH₃COONa, NaHCO₃, Na₂CO₃, and CO₂ (see below for the loading
97 procedure of CO₂ gas). A summary of each solution with the values of parameters used is given in Table 1. All solutions
98 were prepared a minimum 12 hours before the experiments and kept at room T all along this period. The solutions
99 analyzed 12 to 24 hours after being prepared are noted hereafter “fresh”, compared to those measured more than one
100 month later, labelled “aged”. pH was measured at room temperature using a glass combined electrode and calculated at
101 elevated T using the HCh software package (Shvarov, 2008).

Table 1. List of hydrothermal solutions. Concentrations are expressed in molality ($\text{mol}\cdot\text{kg}_{\text{H}_2\text{O}}^{-1}$)

# SOL	pH _{25°C}	W from	W from	HCl	NaCl	NaOH	NaHCO ₃	Na ₂ CO ₃	CH ₃ COOH	HCOOH	CH ₃ COONa	CO ₂ (mbar)	NH ₄ Cl
		Na ₆ W ₁₂ O ₃₉ · H ₂ O	Na ₂ WO ₄ · 2H ₂ O										
1	1.10	0.1		0.1									
2	6.87		0.1	0.1									
2.2	7.06		0.2	0.1									
3	0.15	0.1		1.0									
5	5.60	0.1			0.1								
6	10.58		0.1		0.1								
8	9.56		0.1		3.6								
9	10.06	0.1				0.1							
10	13.02		0.1			0.1							
10.1	13.03		0.01			0.1							
10.2	12.94		0.05			0.1							
10.3	12.98		0.2			0.1							
11	8.90		0.1				1.1						
11.1	7.50		0.1				0.1						
11.2	8.32		0.05				0.1						
11.3	8.31	0.05					0.1						
12	7.2		0.1									151	
12.1	7.2	0.1										199	
13	11.85		0.1					1.2					
R1	4.00		0.1						0.5				
R1.2	2.75	0.1							0.5				
R2	3.00		0.1							0.5			
R2.2	2.00	0.1								0.5			
R3	9.00		0.1								0.5		
R3.2	7.80	0.1									0.5		
N1	7.12		0.1										1.05

102 2.2. Spectroscopic cell and Raman data acquisition

103 Solutions must be contained in a material that satisfies several constraints to obtain high-quality Raman spectra.
104 First, the cell material must have sufficient mechanical resistance at the experimental T-P conditions. Second, it must be
105 transparent in the visible spectral region, and it must not induce fluorescence. Third, the cell material must be chemically
106 inert when in contact with aqueous solutions and must not generate catalytic or redox processes. Fused silica capillary
107 capsules (FSCC) satisfy all these requirements (Chou et al., 2008; Caumon et al., 2013; Dargent et al., 2013; Truche et
108 al., 2014). The capillaries were purchased from Polymicro Technologies, LCC, with an internal diameter of 100 μm and
109 an external diameter of 320 μm . The sample loading procedure includes the following steps: (1) the silica tube was sealed
110 at one extremity using an H₂-O₂ micro torch (Elmaflame), (2) the solution (Table 1) was loaded from the open end of the

111 tube and centrifuged towards the closed end at 12000 rpm, (3) the open end of the tube was connected to a vacuum line,
112 then immersed into liquid nitrogen to freeze the solution, and the atmosphere above the frozen solution was evacuated,
113 (4) CO₂ gas (when needed) was loaded cryogenically, and (5) the open end of the capillary was sealed using a hydrogen
114 flame, while the closed end was kept frozen in liquid nitrogen under vacuum. The pressure of CO₂ loaded cryogenically
115 is estimated to be 10 bar at 20 °C. The partial gas pressure was calculated from the pressure drop in the source reservoir.
116 The method accuracy was considered to be within 20 %, based on volume errors and pressure uncertainty.

117 A heating-stage dedicated to capillary heating at saturated vapour pressure (®CAP-500 Linkam) was used to
118 reach the experimental T, with an accuracy of ±0.1 °C in the range of 20 – 400 °C. The heating stage was coupled with a
119 Raman spectrometer (Labram HR, ®Jobin-Yvon, Horiba) and an optical microscope (®Olympus). The best compromise
120 combining the highest intensity of the ν₁ Raman band of the tungstate ion and the best rejection of silica-glass spectrum
121 was obtained using a 20× magnification and a 500 μm diameter for the confocal hole. Using a grating of 1800 grooves
122 per mm, the 800 mm focal distance of the spectrometer and the 100 μm slit width, a spectral resolution of 0.5 cm⁻¹ is
123 obtained. The 514.532 nm line of an Ar⁺ laser (spectra physics, ®Newport Corporation) was used, with a laser power of
124 70 mW. The spectra were collected in the spectral interval between 150 cm⁻¹ and 4500 cm⁻¹, after 60 s acquisition time
125 per spectral window and four accumulations. The measurements were performed first at room temperature (22±1 °C,
126 without considering laser heating) and from 100 °C, up to 400 °C by step of 100 °C at a heating rate of 10°C·min⁻¹ for
127 each solution coexisting with a vapour phase below the critical point.

128 2.3. Fitting procedure of the Raman spectra

129 We used commercial software ®LabSpec 5.64.15 and ®OriginPro9 to determine peak position, intensity, area, and
130 shape factor for each component in the liquid phase. After baseline subtraction, the decomposition was made using a
131 pseudo-Voigt function (a linear combination of Gaussian and Lorentzian functions). Dissolved W species have Raman
132 bands localized in the 860-1010 cm⁻¹ wavenumbers region. The wavenumbers were constrained before the fitting
133 calculation at the maximum intensity of the different band components of the W species in the 860-1010 cm⁻¹ region.
134 After baseline correction, each Raman peak was integrated (*A_i*) and normalized to the area of the O–H bending band of
135 water (*A_{H2O}*) between 1450 and 1850 cm⁻¹. Fig. 1 displays typical raw Raman spectra of W-bearing solutions obtained
136 at T ranging from 25 to 400 °C. A zoom on the wavenumber domain corresponding to the symmetric stretching (W=O)
137 vibrations is also shown in this figure.

138 The tungstate (WO₄²⁻, hereafter noted “B”) concentration was calculated using calibration equations established
139 from measurements in four strongly alkaline solutions having total W concentrations ranging from 0.01 to 0.2 m. In the
140 860-1010 cm⁻¹ spectral region, where the presence of W species may be identified, the Raman spectra collected with these
141 standard solutions display a single symmetric band at around 927 cm⁻¹, without any additional features that might suggest
142 the presence of other complexes (Figs. 2A, B).

143 We used a linear relationship (Eq. 1) between the volumetric concentration of tungstate (*C_i*, mol·L⁻¹) and its H₂O-
144 normalized Raman band area (*A_i*) to determine the calibration coefficient (*K_i*, see Appendix A, Table A.1, Figs. A1.1, .2)
145 of this species at a given T (Figs. 2C, D).

$$146 \quad C_i = K_i(T) \times A_i \quad (1)$$

147 The calibration coefficient (K_i) depends on the Raman cross-section of the considered band and the spectrometer
148 response. The tungstate volumetric concentration at each investigated T was previously derived according to Eq. 2
149 (Appendix B, Tables B.1-10):

$$150 \quad C_i = (\rho_{\text{fluid}}/F) \times m_i \quad (2)$$

151 where m_i is the molality of tungstate ($\text{mol}\cdot\text{kg}_{\text{H}_2\text{O}}^{-1}$), F the molality to molality conversion factor $F= 1000/(1000-b)$ where
152 b is the mass in grams of total dissolved solutes per 1 kg of liquid, and ρ_{fluid} the density ($\text{g}\cdot\text{cm}^{-3}$) of aqueous solution at a
153 given T and vapour saturation pressure. The density was measured at 25 °C and 1 bar by weighing 1 ml of each solution.
154 The knowledge of the density at high temperature necessitated computational models because we had no control over
155 volumetric variations of the solution inside the FSCC during heating. For this purpose, we compared the soWat model
156 (Driesner and Heinrich, 2007; Driesner, 2007) with the AqSo-NaCl model (Bakker, 2018). These two models require (i)
157 the calculation of NaCl mole fraction, according to Eq. 3:

$$158 \quad x_{\text{NaCl}} = \text{mol}_{\text{eqNaCl}} / [\text{mol}_{\text{eqNaCl}} + (1000-b)/u_{\text{H}_2\text{O}}] \quad (3)$$

159 where b is the mass in grams of total dissolved solutes per 1 kg of liquid and $u_{\text{H}_2\text{O}}$ is the molecular mass of water, and (ii)
160 the pressure value of the solution at each investigated T: 1, 0.9, 15, 85.83 and 220 bar for T = 25, 100, 200, 300 and 400
161 °C, respectively. Both methods gave the same results at the second decimal level (Appendix B, Tables B.1-10).

162 The obtained calibration coefficients for species B at T ranging from 25 to 400 °C (Figs. 2C, D) allows us to
163 quantify its concentration in all solutions and estimate the concentration of the other W species thanks to the following
164 procedure. First, in all the collected Raman spectra, we identified those displaying only one Raman band in addition to
165 that of tungstate (at 927 cm^{-1}) in the $860\text{-}1010 \text{ cm}^{-1}$ spectral region. This configuration existed only under circum-neutral
166 to mid-alkaline conditions - the C species being the only secondary Raman band contribution. Second, we derived the W
167 concentration belonging to the C species by subtracting the previously calculated tungstate concentration (B-species)
168 from the total W concentration of the solution. Third, we inferred the calibration coefficient (k_c) for the C species at T
169 ranging from 25 to 400 °C and calculated the W concentration of C species in all our solutions. Finally, we repeated this
170 step-by-step procedure for Raman spectra displaying three and eventually four Raman bands in the $860 - 1010 \text{ cm}^{-1}$
171 spectral region. Of course, uncertainty increased over the course of this approach because of growing cumulative errors
172 and because some calibration lines were poorly constrained (Appendix C - Tables C.1-3).

173

174 3. Results

175 A total of 5 different Raman bands were detected in the $860 - 1010 \text{ cm}^{-1}$ spectral region, which corresponds to
176 the symmetric stretching ($\text{W}=\text{O}$) vibration domain. This latter domain is overlapped by the asymmetric stretching ($\text{W}=\text{O}$)
177 vibration domain ranging from 825 to 930 cm^{-1} . These Raman bands are identified with alphabetic letters (A, B, C, D, E)
178 and ranked by increasing wavenumbers in the following sections. The corresponding W-species include simple dissolved
179 ions, clusters and polyanion species, like heteropoly acids with keggings structures known as heteropolytungstates. We
180 discuss their respective Raman band attribution in section 4.1.

181

182 3.1. Effect of temperature and pH on W speciation

183 Fig. 3 shows four series of Raman spectra corresponding to four different W-bearing aqueous solutions collected
184 at different pH conditions and T ranging from 25 to 400 °C. Under strongly alkaline conditions (Fig. 3A), only one single
185 Raman band exists in the 860 - 1010 cm^{-1} spectral region at each investigated T. This band noted “B” is identified by its
186 intense and sharp features at $\sim 923 \text{ cm}^{-1}$ at 25 °C, which slightly shifts toward lower frequencies with increasing T. Under
187 acidic to circum-neutral conditions, W speciation is far more complex, with up to five well-identified Raman bands
188 coexisting over the investigated T range. The relative evolution of the area of these bands reflects the evolution of the
189 speciation of tungsten.

190 The Raman band noted “A” is characterized by a broad and weakly intense peak at $\sim 894 \text{ cm}^{-1}$. At room T, this
191 band exists in solution from strongly acidic to neutral conditions (Fig. 3B-D), and its area normalized to the water bending
192 band slightly increases over the 1.1 to 6.9 pH range. The intensity of this “A” band decreases with T and vanishes at T
193 above 200 °C. The Raman band noted “B”, previously identified under alkaline conditions, exists over all the investigated
194 pH and T ranges. Still, its intensity decreases abruptly under circum-neutral pH conditions and remains very low under
195 acidic conditions. The Raman band noted “C” is identified by an intense and sharp peak at $\sim 960 \text{ cm}^{-1}$ at room temperature.
196 Its intensity is maximum under circum-neutral conditions, but it decreases rapidly with increasing pH and disappears at
197 a pH around 11. However, the intensity of this “C” band only slightly decreases under acidic conditions and remains
198 significant even at a pH below 1 at room T. A slight wavenumber shift toward lower values with increasing T is also
199 observed for this band. The Raman band noted “D” appears at a pH below 7 at room temperature. It is characterized by
200 an intense and sharp peak at $\sim 970 \text{ cm}^{-1}$, downshifting toward slightly lower wavenumbers as T increases. This band is
201 the most intense of all at pH values below 7 and a temperature of 25 °C. It remains detectable in solution at T up to 400
202 °C, but a fifth band (noted “E”) progressively replaced it at $T \geq 200 \text{ °C}$. This latter band is well identified by a sharp and
203 intense peak at $\sim 988 \text{ cm}^{-1}$ at 200 °C, downshifting to $\sim 983 \text{ cm}^{-1}$ at 400 °C. At a pH below 2 and $T > 200 \text{ °C}$, precipitation
204 occurs, and no more dissolved W-species remains detectable.

206 3.2. Stability and reversible formation of polytungstates

207 The question of the stability and reversibility of the previously described W speciation was addressed in three
208 different ways: 1) by comparing Raman spectra acquired immediately after heating the capillary at 200, 300, and 400 °C
209 with those obtained at the same temperature after forty-eight hours of pre-heating at 350 °C, 2) by performing heating
210 and cooling cycles, and 3) by measuring W speciation at 25 °C two months after having heated the capillary to 400 °C
211 and by comparing the obtained Raman spectra with both fresh and aged (after six months) unheated solutions.

212 Fig. 4 shows one example of these tests performed on a capillary containing a solution at 0.1 m total W
213 concentration from Na_2WO_4 and 0.5 m acetic acid (#R1), having a pH = 4 at 25 °C, and thus being demonstrative of the
214 evolution of the five previously described Raman bands. The comparison of the Raman spectra obtained at 200, 300, and
215 400 °C immediately after loading the capillary (Fig. 4A, lower part) and after 48 hours of pre-heating at 350 °C (Fig. 4B)
216 are perfectly identical in terms of peak feature (Full Width at Half Maximum FWHM and Gravity Center of the band)
217 and peak intensities (Maximum Height), when normalized to water bending (see Appendix D – Table D). The W
218 speciation is also fully reversible upon heating-cooling cycles over the 200 - 400 °C T range. The D and E Raman bands
219 observed at 200 °C and 300 °C disappear in favour of species C at 400 °C. These two first tests demonstrate that the four

220 Raman bands B, C, D and E belong to four different W species. They also show that these four species are stable and that
221 the equilibrium is achieved within minutes under hydrothermal conditions. However, the third test, which consists of
222 comparing Raman spectra obtained at room T with i) freshly prepared, ii) aged, and iii) heated up to 400 °C solutions,
223 shows a different picture (Fig. 4A). In particular, the species E, not present in the fresh solution, remains abundant in the
224 solution immediately or two months after cooling. Species C, which was present in the initial solution, is absent after
225 cooling, and the abundance of species D is different before and after heating/cooling. Note that W speciation at 25 °C in
226 the unheated solution remains nearly identical in the freshly prepared solution and after six months of ageing. This latter
227 comparative test demonstrates that W-speciation does not reflect equilibrium as observed on the initial solution. The
228 freshly-prepared W-bearing solution is in a metastable equilibrium state. Equilibrium would require more than six months
229 to be reached at 25 °C, species E being the thermodynamically stable by-product of the D (and probably C) species
230 decomposition in solution. It should be noted that species B, C, D and E are present in the system even at ten times lower
231 W-concentration (0.01 m total W concentration; Fig. 5).

232 3.3. Effect of carbonate and chloride ligands

233 The effect of carbonate on W-speciation was studied using three contrasting carbonate-bearing systems, where
234 either CO₂(aq) (solution #12, pH_{25°C} = 7.2), HCO₃⁻ (solution #11, pH_{25°C} = 8.3), or CO₃²⁻ (solution #13, pH_{25°C} = 11.9)
235 were the dominant dissolved carbonate species. At room T, the in-situ pH value of the W-bearing solution (0.1 m
236 Na₂WO₄) in equilibrium with 0.15 bar CO₂(g) was estimated using HCh software package (Shvarov, 2015), based on the
237 relative abundance of HCO₃⁻ and CO₂(aq). The Raman spectra shown in Fig. 6 are strictly identical to those obtained
238 under similar pH and T conditions without carbonate (see Fig. 3). Thus, the presence of dissolved carbonate in a
239 substantial amount (> 0.1 m) has no effect on W speciation over the 6 < pH < 12 and 25 ≤ T ≤ 400 °C ranges.

240 The effect of chloride on W speciation was examined through three solutions in the presence of 0.1 to 3.6 m
241 NaCl. Fig. 7 shows the Raman spectra collected for two different W-bearing solutions containing 3.5 m NaCl, at different
242 pH_{25°C} values: 5.3 and 9.6, respectively. In both systems, chloride complexation with dissolved W species does not occur,
243 as no new species are detected in the solution other than those already described. Under slightly acidic condition (Fig.
244 7A), W speciation remain identical to the one measured in solution #5 (low chloride content and pH_{25°C} = 5.6), up to 300
245 °C. At high salinity (Fig. 7), the presence of species “C” seems to be promoted in comparison with the chloride-low
246 solutions conducted under similar pH conditions (i.e. solutions #5 and #6; Fig. 3).

247 4. Discussion

248 4.1. Identification of W-species

249 Among the five previously detected Raman bands, only the one at 927 cm⁻¹ belonging to species “B”, may be
250 assigned with certainty to the ν_s(W=O) symmetric stretching vibration of the WO₄²⁻ anion (Ng and Gulari, 1984; Bilal et
251 al., 1986; Vigasina et al., 2000; Barré et al., 2005; and Redkin and Bondarenko, 2010). Note that the ν_{as}(W=O) asymmetric
252 stretching mode at 834 cm⁻¹ and the δ(W=O) bending mode at 326 cm⁻¹ of WO₄²⁻ are hindered by the Raman bands of the
253 silica-glass of the FSCC. The other four observed bands (at ~890, 955, 970 and 985 cm⁻¹) are much more difficult to
254 assign to a specific W species as there is no consensus in the literature. However, one crucial finding of this study is that
255 all the detected species under hydrothermal conditions exist in solution at room temperature, even species “E” that forms

256 upon heating at $T \geq 200^\circ\text{C}$ but remains stable two months after cooling at room temperature. Thus, the observed W-
257 species are not specific to the hydrothermal condition. They must have been described in the plethora of studies dedicated
258 to W speciation at ambient condition.

259 In an attempt to propose a first comprehensible identification of these W-species, we cross-compare the
260 published Raman spectroscopic studies (Appendix E - Table E.1) with other sources of W speciation data: potentiometric
261 titration, solubility experiments, ultracentrifugation, mass spectrometry, Nuclear Magnetic Resonance (Appendix E -
262 Table E.2), and thermodynamic calculations (Appendix E - Table E.3). This exercise allows us to infer the most probable
263 W species associated with each Raman peak previously observed. At W concentration above 0.01 m, there is a large
264 consensus in the literature (see recent review by Gumerova and Rompel, 2020) that when an aqueous solution of tungstate
265 is acidified, condensation reactions lead to the formation of polytungstates.

266 **Species “A” - Raman band at 888-892 cm^{-1} .** The morphology of this Raman band is very different from the
267 others: low intensity and very large full-width at half maximum (averaged FWHM are 24, 18 and 14 cm^{-1} at 25 $^\circ\text{C}$, 100
268 $^\circ\text{C}$ and 200 $^\circ\text{C}$, respectively). This Raman band is only detected at $T \leq 200^\circ\text{C}$ and $\text{pH} < 8$. It is always associated with
269 the presence of the “D” and/or “C” bands, and its normalized intensity varies accordingly with these latter bands. The
270 Raman spectra of Keggin hetero-polytungstate anions exhibit bands between 950 and 1015 cm^{-1} ($\nu_s(\text{W}=\text{O})$ symmetric
271 stretching mode) and 825-930 cm^{-1} ($\nu_{as}(\text{W}=\text{O})$ asymmetric stretching mode) as well as bands at lower wavenumbers
272 arising from the bridging W-O-W bonds (Ross-Medgaarden and Wachs, 2007). Thus, this later behaviour leaves us
273 thinking that the “A” band corresponds to the weak asymmetric stretching (W=O) vibrational mode of species “D” and
274 “C”.

275 **Species “C” – Raman band at 950-960 cm^{-1} .** This band is sharp and intense. It is located next to WO_4^{2-} (species
276 “B”), with a slight upshift in wavenumbers. It exists at all investigated T and $\text{pH}_{25^\circ\text{C}} < 10.5$. Its maximum intensity is
277 reached at $\text{pH}_{25^\circ\text{C}} \sim 7$ and room T. The species “C” may coexist alone with WO_4^{2-} at $7 < \text{pH}_{25^\circ\text{C}} < 10.5$ and at T up to 400
278 $^\circ\text{C}$ (Fig. 3C). At $T > 300^\circ\text{C}$, it forms at the expense of species E (and D to a lesser extent) and its formation at elevated T
279 is fully reversible upon cooling. Redkin and Bondarenko (2010) assumed this band to be related to the vibration of
280 $[\text{HW}_6\text{O}_{21}]^{5-}$, by analogy with thermodynamic simulations relying on data reported by Baes and Mesmer (1976) and
281 Wesolowski et al. (1984). In their extensive potentiometric investigation of W(VI) speciation at 300 $^\circ\text{C}$, Wesolowski et
282 al. (1984) considered several criteria to select three speciation schemes compatible with their data. Among the three
283 speciation schemes, two including $[\text{W}_7\text{O}_{24}]^{6-}$ were proposed, but slight preference was given to that comprising the two
284 hexamers $[\text{HW}_6\text{O}_{21}]^{5-}$ and $[\text{W}_6\text{O}_{19}]^{2-}$ in addition to monomers and the dodecamer $[\text{H}_2\text{W}_{12}\text{O}_{40}]^{6-}$. The inclusion of hexameric
285 or heptameric species in their speciation scheme under weakly acidic conditions is debatable. Indeed, since the pioneering
286 work of Jander et al. (1929), the hexameric anion has been included in nearly all speciation models. However, such a
287 choice was unequivocally removed by the combined results of NMR (Maksimovskaya and Burtseva, 1985; Hasting and
288 Howarth, 1992), potentiometric (Cruywagen and Van Der Merwe, 1987), cyclic voltammetric (Himeno et al., 2000), and
289 Raman (Fuchs and Flindt, 1979; Himeno et al., 2000) studies. All these works favour the existence and stability of
290 $[\text{W}_7\text{O}_{24}]^{6-}$ in this pH domain. This species displays a strong $\nu_s(\text{W}=\text{O})$ symmetric stretching Raman band at $\sim 953 \text{ cm}^{-1}$
291 at room temperature (Fuchs and Flindt, 1979; Himeno et al., 2000; Weiner et al., 2005). A comparison of the Raman
292 spectrum of $[\text{W}_7\text{O}_{24}]^{6-}$ in the solid-state (isolated as a piperidinium salt) and a freshly acidified tungstate solution led to
293 the identification of $[\text{W}_7\text{O}_{24}]^{6-}$ in solution (Fuchs and Flindt, 1979). A remarkable similarity was noted between the
294 infrared spectra of heptamolybdate salts and the spectra of $[\text{W}_7\text{O}_{24}]^{6-}$ in solution (Pope, 1983). Maksimovskaya and
295 Burtseva (1985), thanks to a ^{17}O and ^{183}W NMR investigation of tungstate solutions, showed the presence of both

296 $[\text{W}_7\text{O}_{24}]^{6-}$ and $[\text{H}_2\text{W}_{12}\text{O}_{42}]^{10-}$. The equilibrium concentrations between these two species depends on temperature and total
297 W concentration. Despite all these lines of evidence, Wang et al. (2020a) recently assigned this Raman band to HWO_4^- ,
298 to comply with the thermodynamic predictions made by Wesolowsky et al. (1984) or Wood and Samson (2000). We
299 disagree with this choice, even if we recognize that this band assignment is tempting, mainly because it satisfies the
300 classical view of W speciation at elevated temperature and the fact that neutral or weakly charged species are favoured
301 under hydrothermal conditions due to the decrease of the dielectric constant of water (e.g. Crerar et al. 1985; Brimhall
302 and Crerar, 1987). Because of polynuclear W ions, the HWO_4^- was never observed by spectroscopic techniques, even at
303 very high dilution (Cruywagen, 1999). The Raman band at $950\text{-}960\text{ cm}^{-1}$ is kept at room T over a wide pH range (from
304 $\text{pH} = 1$ to nearly 10), and its main features (i.e. position and FWHM) do not change with T. This key observation
305 contradicts the existence of HWO_4^- , a species never reported in such conditions. Therefore, we assigned the Raman band
306 at $\sim 953\text{ cm}^{-1}$ to $[\text{W}_7\text{O}_{24}]^{6-}$ (paratungstate-A).

307 **Species “D” – Raman band at $970\text{-}979\text{ cm}^{-1}$.** At room temperature and a $\text{pH} < 6$, this band is the most intense
308 of all. Its intensity strongly decreases at $T \geq 200\text{ }^\circ\text{C}$ but remains detectable up to $400\text{ }^\circ\text{C}$ under acidic conditions ($\text{pH} <$
309 5). The disappearance of this band at elevated T is not reversible upon cooling (Fig. 4). Therefore, the species “D” is
310 metastable. Bilal et al. (1986) assigned this band to the $[\text{W}_{10}\text{O}_{32}]^{4-}$ species (tungstate-Y) in their Raman spectra recorded
311 at $150\text{ }^\circ\text{C}$, 1 kbar and $\text{pH}_{150\text{ }^\circ\text{C}} = 6$. These authors also observed the complete disappearance of this band at $T = 200\text{ }^\circ\text{C}$.
312 This behaviour is in good agreement with our observations. Tungstate-Y is known to be kinetically unstable in aqueous
313 solutions (Gumerova and Rompel, 2020). Upon prolonged heating at $80\text{ }^\circ\text{C}$, it yields the thermodynamically stable true
314 α -metatungstate $\alpha\text{-}[\text{H}_2\text{W}_{12}\text{O}_{40}]^{6-}$ (Hasting and Howarth, 1992; Himeno and Kitazumi, 2003). Thus, we assigned the
315 Raman band at $970\text{-}979\text{ cm}^{-1}$ to $[\text{W}_{10}\text{O}_{32}]^{4-}$ (tungstate-Y).

316 **Species “E” – Raman band at $983\text{-}995\text{ cm}^{-1}$.** This band is very sharp (averaged FWHM are 7, 6, and 2 cm^{-1} at
317 $200, 300,$ and $400\text{ }^\circ\text{C}$, respectively) and intense. It only appears at a $\text{pH} \leq 7$ and $T \geq 200\text{ }^\circ\text{C}$ upon heating. It forms at the
318 expense of species “D”. The behaviour of the species corresponding to this band is surprising since its formation is
319 reversible upon heating and cooling in the $200 - 400\text{ }^\circ\text{C}$ T range. Once formed, it remains stable at room temperature
320 even after two months (Fig. 4). This band was assigned to the $[\text{W}_{10}\text{O}_{32}]^{4-}$ by Himeno et al. (2000) in their Raman spectra
321 obtained at room T and a $\text{pH} < 4$, without heating. They observed the band disappearance upon increasing the pH above
322 3 or after heating at $80\text{ }^\circ\text{C}$ for three days. This behaviour is inconsistent with our observations: species E forms upon
323 heating preferentially under slightly acidic conditions. Thus, we rule out the possibility for $[\text{W}_{10}\text{O}_{32}]^{4-}$ to belong to this
324 Raman band at $983\text{-}995\text{ cm}^{-1}$. This band was assigned to $[\text{H}_3\text{W}_{12}\text{O}_{40}]^{5-}$ by Bilal et al. (1986) in their spectra recorded at
325 $150\text{ }^\circ\text{C}$, 1 kbar and $\text{pH}_{150\text{ }^\circ\text{C}} = 6$. These authors also observed that this complex is the only stable polymeric species at a
326 $\text{pH} < 5$, $T = 200\text{ }^\circ\text{C}$ and $P = 1\text{ kbar}$. Again, this observation is in excellent agreement with our measurements. Other minor
327 species (mainly B and D) may be attributed to lower pressure (vapour saturation pressure) or a better sensitivity of our
328 spectrometer. Wang et al. (2020a) also detected this band in their experiments performed from 0.03 to $0.1\text{ mol kg}_{\text{H}_2\text{O}}^{-1}$ of
329 total W concentration in the presence of CO_2 . Still, they did not assign it to a particular polymeric species. In their
330 thorough and comprehensive NMR spectroscopy study (^{183}W , ^{17}O and ^1H) of tungstate solution in the pH range 1.5 to 8,
331 Hasting and Howarth (1992) gave an in-depth perspective on the formation of W species in solution based on poly-
332 oxoanions already characterized in the solid-state. The $[\text{H}_3\text{W}_{12}\text{O}_{40}]^{5-}$ polyanions is a protonated form of paratungstate-B
333 ($[\text{H}_2\text{W}_{12}\text{O}_{42}]^{10-}$) that forms at $\text{pH} < 2$. This description does not correspond to our observations because species E appears
334 at $T > 100\text{ }^\circ\text{C}$ and slightly acidic conditions. Thus, $[\text{H}_3\text{W}_{12}\text{O}_{40}]^{5-}$ and $[\text{W}_{10}\text{O}_{32}]^{4-}$ complexes cannot be assigned to the
335 Raman band at $983\text{-}995\text{ cm}^{-1}$. Instead, the well-known behaviour of α -metatungstate ($\alpha\text{-}[\text{H}_2\text{W}_{12}\text{O}_{40}]^{6-}$) which is the

336 dominant and thermodynamically stable W-species that forms upon prolonged heating (70 °C) below pH 6 (Hasting and
337 Howarth, 1992; Himeno et al., 2000, Himeno et Kitazumi, 2003) satisfies all our observations. Therefore, we assigned
338 the Raman band at 983-995 cm⁻¹ to α -[H₂W₁₂O₄₀]⁶⁻ (α -metatungstate).

339 Sodiated tungstate species were never reported in the literature (see review by Gumerova and Rompel, 2020),
340 and a recent (preliminary) XAS investigation under hydrothermal conditions tends to confirm the absence of sodiation
341 (Klemme et al., 2021). Salts containing fragments of heptatungstate structure, Na₅[H₃W₆O₂₂] (Hartl et al., 1993), were
342 isolated from concentrated weakly acidic aqueous solutions, but there is no evidence that this anion is stable in solution.
343 The fact that protonated and non-protonated polytungstate species may coexist simultaneously and non-protonated species
344 may even dominate W speciation under very acidic conditions relies on experimental data reported by numerous studies
345 (see Gumerova and Rompel, 2020 for a review). Part of this observation may be explained by the enthalpy factor of the
346 condensation process and by the metastability of some anions. However, DFT calculations are definitively needed to
347 solve this critical question.

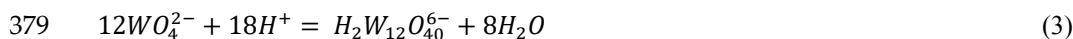
348 4.2. Tungsten speciation

349 Based on our calibration procedure, we were able to derive the concentration of WO₄²⁻ and to estimate step by
350 step the concentration of the three other identified species, namely [W₇O₂₄]⁶⁻, [W₁₀O₃₂]⁴⁻, and α -[H₂W₁₂O₄₀]⁶⁻ in all our
351 solutions at each temperature up to 400 °C. The obtained calibration coefficient (K_T) values are within the 0.01 to 0.2
352 mol.L⁻¹ range. Surprisingly, the tungsten polymerization does not significantly affect the value of the Raman scattering
353 coefficients. These coefficients tend to decrease with temperature starting from about 0.15 mol.L⁻¹ at 25 °C and decreasing
354 abruptly to 0.02 – 0.04 mol.L⁻¹ at T > 200 °C. Only the calibration coefficient of the [W₇O₂₄]⁶⁻ species displays a
355 significantly different behaviour, with a slight increase with T from 0.15 to 0.2 mol.L⁻¹ over the 25 – 400 °C T range. The
356 solution pH was measured at room temperature and then calculated at elevated temperature using the the HCh software
357 package (Shvarov, 2008). This approach is relatively safe under extreme pH conditions (pH < 3 or pH >10) or in the
358 presence of concentrated pH buffers (acetic acid, formic acid, carbonate/bicarbonate solutions) because the evolving
359 tungsten speciation weakly impacts H⁺ activity. However, for a small number of solutions (e.g. sol.#2, #2.2 and #5) where
360 the circum-neutral pH conditions measured at ambient conditions were not buffered, our calculations were made for the
361 indicative purpose as there is no thermodynamic data available a priori for the observed complex at elevated temperature.
362 The resulting tungsten speciation as a function of pH is shown in Fig. 8 at 25, 100, 200, and 300 °C.

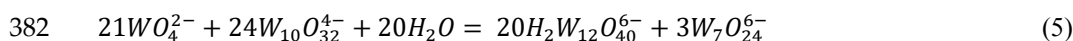
363 The WO₄²⁻ anion is the predominant species at a pH above 7.5 and T = 25 °C. Its predominance domain is slightly
364 shifted toward a lower pH value with increasing temperature. Interestingly, we detected and quantified the presence of
365 WO₄²⁻ even under strongly acidic conditions, where it still represents between 5 to 10 % of the total dissolved W
366 concentration. The [W₇O₂₄]⁶⁻ polyanion is the predominant species under circum-neutral conditions (6 < pH < 7) at T up
367 to 100 °C. This latter species still represents an essential contribution to the W speciation (20 to 40 %) at lower pH. At
368 higher T, its concentration in solution drastically decreases, and it only represents 10 to 20 % of the total dissolved W
369 concentration. The [W₁₀O₃₂]⁴⁻ polyanion, which is metastable, dominates the W speciation at pH < 5 and T up to 200 °C
370 upon heating. Under these conditions, its concentration represents 40 to 80 % of the total W speciation. Upon further
371 heating [W₁₀O₃₂]⁴⁻ progressively disappears in favour of α -[H₂W₁₂O₄₀]⁶⁻. The disappearance of [W₁₀O₃₂]⁴⁻ is not reversible
372 upon cooling. Finally, the α -[H₂W₁₂O₄₀]⁶⁻ polyanion is the most abundant and stable species at pH < 6 and T ≥ 300 °C.
373 Once formed, α -[H₂W₁₂O₄₀]⁶⁻ remains in solution upon cooling, which is not the case for [W₁₀O₃₂]⁴⁻.

374 4.3. Thermodynamic calculations

375 Raman spectroscopy data on W speciation obtained in this study were used to calculate the stability constants of
376 W polymers. The following reactions describe their formation from WO_4^{2-} :



380 Besides, the following pH-independent reactions can be written:



383 The most important W polymers (~50% of dissolved W) coexisting with high amounts of WO_4^{2-} (~50% of
384 dissolved W) under our experimental conditions are $[W_7O_{24}]^{6-}$ at 25 – 100 °C and α - $[H_2W_{12}O_{40}]^{6-}$ at 200 - 300 °C. The
385 experimentally determined concentrations (in mol·kg_{H₂O}⁻¹) of these polymers and WO_4^{2-} together with the corresponding
386 estimated pH values were used to calculate the apparent constants for the reactions 1 and 3 according to:

$$387 \quad \log_{10}K_m(1) = \log \frac{m(W_7O_{24}^{6-})}{[m(WO_4^{2-})]^7} + 8pH \quad (6)$$

$$388 \quad \log_{10}K_m(3) = \log \frac{m(H_2W_{12}O_{40}^{6-})}{[m(WO_4^{2-})]^{12}} + 18pH \quad (7)$$

389 At 25°C and pH above 6.5, a good consistency between the pH and WO_4^{2-} and $[W_7O_{24}]^{6-}$ concentrations were
390 found for all solutions except that under high NaCl concentration (3.6 m NaCl). We expect this to be caused by the
391 increased uncertainty in classical pH measurements at high NaCl concentrations. Thus, this point was excluded from the
392 analyses. For the other experiments at pH 6.5 - 8.5, the pH values within ± 0.3 uncertainty were described by the apparent
393 constant $\log_{10}K_m(1)$ value 67.1 ± 1.5 calculated according to equation (6). At pH below 6.5, the equilibrium between
394 WO_4^{2-} and $[W_7O_{24}]^{6-}$ does not seem to be reached, i.e. there is no stable relationship between the pH value and WO_4^{2-} and
395 $[W_7O_{24}]^{6-}$ concentrations. The pH-independent reaction (4) was calculated as:

$$396 \quad \log_{10}K_m(4) = \log \frac{[m(W_7O_{24}^{6-})]^2}{[m(WO_4^{2-})]^4 \cdot m(W_{10}O_{32}^{4-})} \quad (8)$$

397 The apparent constant $\log K_m(4)$ was found to be 5.4 ± 1.0 for all solutions at 25 °C. A similar analysis of W polymers
398 formation was done at 100 °C. The corresponding constant is given in Table 2.

399 At 200 - 300 °C, α - $[H_2W_{12}O_{40}]^{6-}$ and WO_4^{2-} distribution in experimental solution as a function of pH can be
400 described by the apparent constants given in Table 2.

401

402 **Table 2. Apparent constants determined in this study**

Reaction		T	$\log K_m$	$I_{m(T)}$	pH_T
$7WO_4^{2-} + 8H^+ = W_7O_{24}^{6-} + 4H_2O$	(1)	25°	67.1 ± 1.5	0.3-0.7	≥ 6.5
		100°C	65.1 ± 1.0	0.3-0.7	≥ 6.5
$4WO_4^{2-} + W_{10}O_{32}^{4-} = 2W_7O_{24}^{6-}$	(4)	25°C	5.4 ± 1.0	0.3-1.2	0.1-5.6
		100°C	5.3 ± 1.2	0.3-1.2	0.1-5.6
$12WO_4^{2-} + 18H^+ = H_2W_{12}O_{40}^{6-} + 8H_2O$	(3)	200°C	116.0 ± 3.5	0.3-0.8	4.5-6.0
		300°C	116.0 ± 1.5	0.3-0.8	4.5-6.0

403

404 The correction to the ionic strength is required to calculate the constants at infinite dilution. For this correction,
405 the extended Debye-Hückel equation was applied:

406 $\log_{10}\gamma_i = -z^2 D = -z^2 \frac{A\sqrt{I_m}}{1+B\alpha\sqrt{I_m}}$ (9)

407 where D is the Debye-Hückel term with A and B parameters which are constant at a given temperature (Appendix F,
408 Table F.1.), and I_m is the ionic strength, calculated as

409 $I_m = 0.5 \cdot \sum_{i=1}^n m_i \cdot z_i^2$ (10)

410 where m_i and z_i are a concentration (in mol·kg_{H2O}⁻¹) and a charge of aqueous species, respectively. The ionic strength was
411 calculated considering the experimental data on W polymer concentrations and assuming all other ions as dissociated.
412 Rather high uncertainties in the pH at elevated temperatures, species concentrations, and ionic strength calculations,
413 together with the use of multiple electrolytes, imply very high uncertainties in activity coefficient calculations. Thus,
414 applying more accurate models of ionic strength correction (e.g. specific ion interaction model or Pitzer model) is
415 meaningless for this study. The extended Debye-Hückel theoretical approach (equation 9) was the most suitable.
416 Constants given in Table 3 were calculated from the apparent constants (Table 2) according to:

417 $\log_{10}K^0(1) = \log \frac{m(W_7O_{24}^{6-})}{[m(WO_4^{2-})]^7} + 8pH - 8D$ (11)

418 $\log_{10}K^0(3) = \log \frac{m(H_2W_{12}O_{40}^{6-})}{[m(WO_4^{2-})]^{12}} + 18pH + 12D$ (12)

419

420 The thermodynamic constants of reactions (1) and (2) at 200 – 300 °C were optimized to better reproduce the experimental
421 distribution of W species. The optimized values of thermodynamic constants are given in Table 3.

422 **Table 3. Thermodynamic constants determined in this study**

Reaction		T	$\log_{10}K^0$
$7WO_4^{2-} + 8H^+ = W_7O_{24}^{6-} + 4H_2O$	(1)	25°C	65.6 ± 1.5
		100°C	62.9 ± 1.5
		300°C	48.8 ± 1.5
$10WO_4^{2-} + 16H^+ = W_{10}O_{32}^{4-}$	(2)	300°C	$107.0 \pm 1.5^*$
$12WO_4^{2-} + 18H^+ = H_2W_{12}O_{40}^{6-} + 8H_2O$	(3)	200°C	119.0 ± 3.5
		300°C	119.0 ± 0.5

423 * this species $[W_{10}O_{32}]^{4-}$ is believed to be metastable (see more discussion in the text).

424

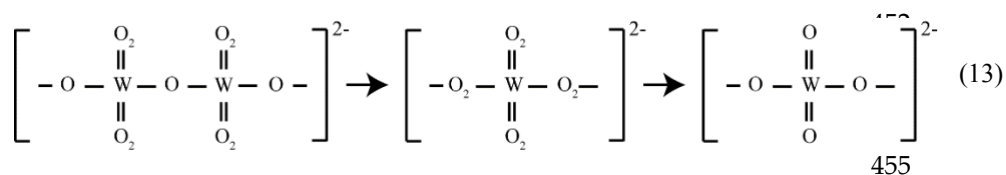
425 The value of $\log_{10}K(1)$ at $T = 25$ °C obtained in this study (65.6 ± 1.5) agrees with the literature data (65.19,
426 Cruywagen and Van Der Merwe, 1987). The values of stability constants of W polymers at high temperatures are
427 determined for the first time. In Fig. 9, the speciation of W at 300 °C in 1 m NaCl solution is calculated for Na₂WO₄-
428 HCl-NaOH-H₂O system as a function of pH based on the data reported in Table 3 and by applying equation (9) for the
429 activity coefficient calculation. The polymer $[W_{10}O_{32}]^{4-}$ is expected to be thermodynamically unstable (see section above).
430 The value of $\log_{10}K(2)$ given in Table 3 allows estimating some theoretical behaviour of this species under equilibrium.
431 When excluding $[W_{10}O_{32}]^{4-}$, the models predict α -[H₂W₁₂O₄₀]⁶⁻ as the dominant W species, under low pH. The
432 predominance of W polymers calculated in Fig. 9A does not change when $[W_{10}O_{32}]^{4-}$ is excluded. Thus, our
433 thermodynamic data can be used for modelling hydrothermal transport of W during ore deposit formation.

434 4.4. Geological implications

435 The evolution of W-speciation is strongly dependent on temperature and pH. Our experimental study
436 demonstrates that W forms highly-charged polymers up to 400 °C like the para-tungstate A (C species) (W₇O₂₄)⁶⁻, which
437 is stable at all investigated temperatures, and the decatungstate Y (D species) (W₁₀O₃₂)⁴⁻. This latter species is metastable

438 and may be replaced by the dodeca α -metatungstate (E species) ($H_2W_{12}O_{40}$)⁶⁻ which forms at $T \geq 200$ °C. Even if these
 439 polymeric species may be considered with caution, they predominate in solution under acidic to circumneutral conditions
 440 at temperatures up to 400 °C. The existence of stable, highly-charged polymeric species at temperatures up to 400 °C is
 441 a significant discovery as it definitively shifts the long-standing paradigm that only neutral or weakly-charged species
 442 predominate under hydrothermal conditions. This is due to the decrease of the dielectric constant of water with the
 443 increasing temperature (Crerar et al., 1985; Mei et al., 2014; Brugger et al., 2016).

444 Moreover, the W species detected at elevated temperatures also exist at ambient conditions with no new complex
 445 or polymers formation. This strong tendency of tungsten to form complexes, like heteropoly-, aquapoly-, and isopoly-
 446 tungsten compounds, is unique. No other element of the periodic table (not even Mo, the W chemical brother) acts in that
 447 way. The contrasting behaviour between W and Mo may be explained by the weakening of bonding of the valence
 448 electrons from Mo to W, resulting in the stability increase of the higher oxidation states of W and its tendency to form
 449 oxygen compounds having Kegging structure. Mo combines with S to precipitate molybdenite, whereas W still forms
 450 oxides like wolframite or scheelite. Equation 13 from Barabanov (1971) shows this strong affinity of W for oxygen in
 451 acidic conditions and its gradual weakening with increasing pH values as observed in the present study.



456 This new view of W speciation under hydrothermal conditions has significant consequences for W transport and
 457 deposition in natural environments by hydrothermal aqueous fluids.

458 The importance of W polymers in ore-forming hydrothermal fluids was modelled according to thermodynamic
 459 data obtained in this study (Table 3) and presented in Fig. 9. The possible input of $HWO_4^-/H_2WO_4^0$ (aq) species was
 460 calculated according to Wang et al. (2019). The inclusion of this species in the model does not significantly change the
 461 speciation of W polymers (see Figs. 9A and 9B). The total W concentration and pH are the main factors controlling the
 462 formation of W polymers in Na_2WO_4 -NaCl-HCl-NaOH system. The acidic pH and high W contents favor W
 463 polymerization (Fig. 9d). Our modeling shows that the concentration of NaCl strongly affects the W speciation due to the
 464 high charge of W polymers (see Fig.F.1.3). For example, the role of highly charged species (i.e. W polymers) increases
 465 with increasing electrolyte concentration. Moreover, the solubility of W minerals is known to increase with increasing
 466 NaCl or KCl concentration (see Redkin and Cygan, 2020 and references cited). In Ca- and Fe-bearing fluids with near-
 467 neutral pH, the low solubility of scheelite $CaWO_4$ and ferberite $FeWO_4$ prevents the formation of W polymers. Under
 468 more acid conditions, the formation of W polymers would favour high solubility, but under pH below 4.5, the fields of
 469 W polymers and WO_3 precipitation overlap (i.e. Fig. 9d). The latter means that the presence of dissolved Ca and Fe in
 470 natural fluids does not favour high W concentrations. Tungsten-ore forming fluids may contain more than 1000 ppm W,
 471 as recently revealed by fluid inclusion studies (Korges et al., 2018). Such high W concentrations reaching the millimolar
 472 range are sufficient to trigger W polymerization, as demonstrated by our in-situ measurements and thermodynamic
 473 calculations (Figs. 5a and 9). Some geological fluids are very rich in W, and a total W concentration of around 2000 ppm
 474 is not unrealistic in natural ore-forming fluids (Table 4). We point out here that most fluid inclusion studies were made
 475 on quartz that is supposed to be coeval with W-bearing minerals. It implies that the entrapped fluids were partly depleted
 476 in W during the ore-forming stage. Despite this phenomenon, these fluids still contain more than 200 ppm of W, and the
 477 original W bearing-fluid was probably even richer in W (Naumov et al., 2011; Goldmann et al., 2013; and Hulsbosch et

478 al., 2016). Korges et al. (2018) revealed via in-situ LA-ICP-MS analysis of fluid inclusions from the Sn-W Zinnwald
 479 deposit in the Erzgebirge (Germany) that ore-forming fluids contained up to 1000 ppm total W concentration. Beuchat et
 480 al. (2004) reported exceptional W enrichment in fluid inclusions from the W-Cu-Zn-Pb San Cristobal district (Peru), with
 481 W concentration exceeding 10,000 ppm in quartz from the early W ore deposition stage.

482

483 **Table 4. W concentrations in natural fluids**

METHODOLOGY	SOURCES	W concentrations from literature						
		Beuchat et al., 2004	Naumov et al., 2011	Hulbosch et al., 2016	Fusswinkel et al., 2017	Zhang et al., 2017	Korges et al., 2018	Guo et al., 2019
LA-ICP-MS and Microthermometric FI studies	Wfm-Qtz-Py Stage	100 < ppm < 10000						
Database Review	Magmatic Melts Mineral-Forming Fluids		6.8 ppm (+81 ppm/-6.2 ppm) 30 ppm (+114 ppm/-25 ppm)					
RAMAN on FI Studies	Ms associate with Sch and Frb Tur associate with pegmatite			3 < ppm < 1310				
LA-ICP-MS in FIA	Early Qtz vein				0.03 < µg/g < 9.9			
LA-ICP-MS in FIA	Late Extensional vein				8.24 < µg/g < 23			
LA-ICP-MS	Two-mica granite					50 < ppm < 70		
LA-ICP-MS in FIA	Wmf-Cst-Qtz						10 < ppm < 10000	
ICP-MS in Active Hydrothermal System	Water samples Sediments nearby the vents							0.05 < µg/L < 1103 6.49 < ppm < 536

Abbreviations Legend

- Sch = scheelite
- Frb = ferberite
- Tur = tourmaline
- Wfm = wolframite
- Qtz = quartz
- Py = pyrite
- Cst = cassiterite
- FIA = fluid inclusion assemblage

484

485 Usually, fluid inclusions associated with quartz-vein type wolframite deposits are commonly accompanied by
 486 the dominant presence of CO₂ (Higgins, 1980; Ball et al., 1985; Wood and Samson, 2000; Rios et al., 2003; Naumov et
 487 al., 2011 and Ni et al., 2015). According to Cathelineau et al. (2020), W-ores at Panasqueira W deposit (Portugal)
 488 precipitated from low salinity, aqueous-carbonic fluids with CO₂ - CH₄ - N₂ present in the volatile phase. Tungsten does
 489 not form complexes with carbonate species over the whole pH and T ranges investigated in the present work. This
 490 observation does not preclude an essential role for CO₂/carbonates in the transport and deposition of W: first, the presence
 491 of dissolved CO₂ may buffer the pH in the range 5 - 6 and thus favours a W speciation dominated by polymeric species.
 492 Second, CO₂/water immiscibility may result in CO₂ degassing and trigger wolframite precipitation due to a pH increase
 493 (Liu et al., 2018, Wood and Samson, 2000; Liu and Xiao, 2020; Wang et al., 2019, 2020b). Third, although pressure has
 494 a secondary effect on the transport and deposition of W-ore minerals, unmixing of CO₂ may indirectly promote the
 495 instability of W species by decreasing water activity and modifying the dielectric constant of the solvent, which controls
 496 ion paring (Kokh et al., 2017). Unmixing is recognized at Panasqueira (Portugal) W-ore deposit but only during the last
 497 stages (noted IV following Cathelineau et al., 2020). Unmixing could have a role on W speciation and subsequently on
 498 the W precipitation, but it does not explain most of the wolframite precipitation at the very beginning of its formation
 499 under high pressure conditions, which excludes any unmixing process during early stages at Panasqueira.

500 **5. Conclusions**

501 The present study was based on in-situ Raman observations of W speciation in aqueous solutions loaded in fused
502 silica capillary capsules (FSCC) at temperatures ranging from 25 to 400 °C and at different pH conditions. We identified
503 four main W-species: (i) the tungstate anion (WO_4^{2-}) which was found to be predominant at pH above 7.5 at 25 °C; (ii)
504 the paratungstate A polyanion ($\text{W}_7\text{O}_{24}^{6-}$), which was found stable under circum-neutral conditions ($6 < \text{pH} < 7$) at $T \leq$
505 100 °C; (iii) the decatungstate Y-polyanion ($\text{W}_{10}\text{O}_{32}^{4-}$), a metastable polyanion, which predominates at a $\text{pH} < 5$ and $T \leq$
506 200 °C upon heating; and (iv) α -metatungstate ($\alpha\text{-}[\text{H}_2\text{W}_{12}\text{O}_{40}]^{6-}$) which was the most abundant species at a $\text{pH} < 6$ and T
507 ≥ 300 °C.

508 Significant findings from this study are summarized below.

- 509 1) In aqueous solutions of highly soluble salts Na_2WO_4 and $\text{Na}_6\text{W}_{12}\text{O}_{39}$, tungsten polymers form reversibly under acidic
510 to circum-neutral conditions and T up to 400 °C with a total tungsten concentration down to 0.01 m (~1700 ppm).
- 511 2) Tungsten does not form complexes with chloride and carbonate ions over the pH and T range investigated here ($0 <$
512 $\text{pH} < 13$, 25 °C $< T < 400$ °C, $0.01\text{m} < W < 0.2\text{m}$).
- 513 3) The W polymers identified under hydrothermal conditions are similar to those already well characterized at room T .
- 514 4) This work shifts the long-standing paradigm that highly-charged polymers cannot exist under hydrothermal conditions
515 because of the decrease of the dielectric constant of water with T increase.
- 516 5) Thermodynamic constants for the three detected polytungstate anions are provided up to 300 °C. Our new data enabled
517 the first quantitative predictions of the abundance of W polymers in geological fluids and allowed us to evaluate their
518 role in W transport and deposition in ore deposits.

519 To constrain both electronic reorganization and nuclear quantum effects associated with oxygen bonding and
520 polymerization, accurate ab initio molecular dynamics (AIMD) models are needed. Predicting the Raman spectra of the
521 detected W polymers using density functional theory (DFT) will be essential for a full attribution of the W polymer
522 Raman bands observed in this study.

523 *Acknowledgements*

524 We warmly acknowledge Associate editor Pr Jean François Boily for his work and the three anonymous reviewers for
525 their very constructive reviews. We are grateful to Maria A. Kokh for her insightful discussion and precious advice along
526 the course of this study. The authors also acknowledge Mr. Christopher Daly for the English verification. Pascal Robert
527 and Aurélien Randi are warmly thanked for their help with the experimental setup. Guillaume Barre and Julien Boulliung
528 are thanked for sharing their experiences and valuable suggestions on capillary loading techniques. Laurent Truche
529 acknowledges support from the Institut Universitaire de France. This work was funded by the ERAMIN project NewOres
530 funded by ANR (ANR-14-EMIN-0001), and Labex Ressources 21 (supported by the French National Research Agency
531 through the national program “Investissements d’avenir”) with reference ANR – 10 – LABX 21 —LABEX
532 RESSOURCES 21.
533

534 **References**

- 535 Arnek, R., & Sasaki, Y. (1974). Equilibrium Studies of Polyanions. 20. A Recalculation of Emf Data on the Reactions of
536 H^+ and WO_4^{2-} in 3 M $Na(ClO_4)$ at 25 °C. *Acta Chem. Scand. A*, 28(1).
- 537 Aveston, J. (1964). Hydrolysis of tungsten (VI): ultracentrifugation, acidity measurements, and Raman spectra of
538 polytungstates. *Inorganic Chemistry*, 3(7), 981-986.
- 539 Baes, C. F., & Mesmer, R. E. (1976). *The Hydrolysis of Cations* Wiley. *New York*, 177-182.
- 540 Bakker, R. J. (2018). AqSo_NaCl: Computer program to calculate pTVx properties in the H₂O-NaCl fluid system applied
541 to fluid inclusion research and pore fluid calculation. *Computers & geosciences*, 115, 122-133.
- 542 Ball, T. K., Fortey, N. J., & Shepherd, T. J. (1985). Mineralisation at the Carrock Fell tungsten mine, N. England:
543 paragenetic, fluid inclusion and geochemical study. *Mineralium Deposita*, 20(1), 57-65
- 544 Barabanov, V. F. (1971). Geochemistry of tungsten. *International Geology Review*, 13(3), 332-344
- 545 Barré, T., Arurault, L., & Sauvage, F. X. (2005). Chemical behavior of tungstate solutions: Part 1. A spectroscopic survey
546 of the species involved. *Spectrochimica Acta Part A: Molecular and Biomolecular Spectroscopy*, 61(4), 551-557.
- 547 Beuchat, S., Moritz, R. and Pettke, T., 2004. Fluid evolution in the W–Cu–Zn–Pb San Cristobal vein, Peru: fluid inclusion
548 and stable isotope evidence. *Chemical Geology*, 210(1-4), pp.201-224.
- 549 Bilal, B. A., Haufe, P., & Möller, P. (1986). Raman spectroscopic and electrochemical study of polymerization of tungsten
550 (VI) in a hydrothermal solution up to 1 kbar and 200 C. *Physica B+ C*, 139, 721-724.
- 551 Brimhall, G.H. & Crerar, D.A., (1987). Ore fluids: magmatic to supergene. In: I.S.E. Carmichael and H.P. Eugster
552 (Editors), *Thermodynamic Modelling of Geochemical Materials: Minerals, Fluids and Melts. Rev. Mineral.*, 17:
553 235-321.
- 554 Brugger, J., Liu, W., Etschmann, B., Mei, Y., Sherman, D. M., & Testemale, D. (2016). A review of the coordination
555 chemistry of hydrothermal systems, or do coordination changes make ore deposits? *Chemical Geology*, 447, 219-
556 253.
- 557 Cathelineau, M., Boiron, M., Marignac, C., Dour, M., Dejean, M., Carocci, E., Truche, L., & Pinto, F. (2020). High
558 pressure and temperatures during the early stages of tungsten deposition at Panasqueira revealed by fluid inclusions
559 in topaz. *Ore Geology Reviews*, 126, 103741.
- 560 Caumon, M. C., Dubessy, J., Robert, P., & Tarantola, A. (2013). Fused-silica capillary capsules (FSCCs) as reference
561 synthetic aqueous fluid inclusions to determine chlorinity by Raman spectroscopy. *European Journal of*
562 *Mineralogy*, 25(5), 755-763.
- 563 Chou I.-M., Song Y. & Burruss R. C. (2008). A new method for synthesizing fluid inclusions in fused silica capillaries
564 containing organic and inorganic material. *Geochim. Cosmochim. Acta* 72, 5217–5231.
- 565 Crerar, D., Wood, S., Brantley, S., & Bocarsly, A. (1985). Chemical controls on solubility of ore-forming minerals in
566 hydrothermal solutions. *Canadian Mineralogist*, 23(3), 333-352.
- 567 Cruywagen, J. J., & Van Der Merwe, I. F. (1987). Tungsten (VI) equilibria: a potentiometric and calorimetric
568 investigation. *Journal of the Chemical Society, Dalton Transactions*, (7), 1701-1705.
- 569 Cruywagen, J. J. (1999). Protonation, oligomerization, and condensation reactions of vanadate (V), molybdate (VI), and
570 tungstate (VI). In *Advances in inorganic chemistry* (Vol. 49, pp. 127-182). Academic Press.
- 571 Dargent, M., Dubessy, J., Truche, L., Bazarkina, E. F., Nguyen-Trung, C., & Robert, P. (2013). Experimental study of
572 uranyl (VI) chloride complex formation in acidic LiCl aqueous solutions under hydrothermal conditions (T= 21
573 C–350 C, Psat) using Raman spectroscopy. *European Journal of Mineralogy*, 25(5), 765-775.

- 574 Driesner, T. (2007). The system H₂O–NaCl. Part II: Correlations for molar volume, enthalpy, and isobaric heat capacity
575 from 0 to 1000 C, 1 to 5000 bar, and 0 to 1 XNaCl. *Geochimica et Cosmochimica Acta*, 71(20), 4902-4919.
- 576 Driesner, T., & Heinrich, C. A. (2007). The system H₂O–NaCl. Part I: Correlation formulae for phase relations in
577 temperature–pressure–composition space from 0 to 1000 C, 0 to 5000 bar, and 0 to 1 XNaCl. *Geochimica et*
578 *Cosmochimica Acta*, 71(20), 4880-4901.
- 579 Duncan, J. F., & Kepert, D. L. (1961). 1050. Polyanion equilibria in aqueous solution. Part I. The quantitative analysis of
580 acidified tungstate solutions. *Journal of the Chemical Society (Resumed)*, 5317-5325.
- 581 Eugster H. P. & Wilson G. A. (1985). Transport and deposition of ore-forming elements in hydrothermal systems
582 associated with granites. In High Heat Production Granites, Hydrothermal Circulation and Ore Genesis. *Inst. Min.*
583 *Metall., London*, pp. 87-98.
- 584 Fuchs, J., & Flindt, E. P. (1979). Preparation and structure investigation of polytungstates-contribution to the
585 paratungstate-a problem. *Zeitschrift für Naturforschung Section Ba Journal of Chemical Sciences*, 34(3), 412-422.
- 586 Fusswinkel, T., Wagner, T., & Sakellaris, G. (2017). Fluid evolution of the Neoproterozoic Pampalo orogenic gold deposit
587 (E Finland): Constraints from LA-ICPMS fluid inclusion microanalysis. *Chemical Geology*, 450, 96-121.
- 588 Gibert, F., Moine, B., Schott, J., & Dandurand, J. L. (1992). Modeling of the transport and deposition of tungsten in the
589 scheelite-bearing calc-silicate gneisses of the Montagne Noire, France. *Contributions to Mineralogy and*
590 *Petrology*, 112(2-3), 371-384.
- 591 Goldmann, S., Melcher, F., Gäbler, H. E., Dewaele, S., Clercq, F. D., & Muchez, P. (2013). Mineralogy and trace element
592 chemistry of ferberite/reinite from tungsten deposits in central Rwanda. *Minerals*, 3(2), 121-144.
- 593 Gumerova, N.I., & Rompel, A. (2020). Polyoxometalates in solution: speciation under spotlight. *Chemical Society*
594 *Reviews*, 49(21), pp.7568-7601.
- 595 Guo, Q., Li, Y., & Luo, L. (2019). Tungsten from typical magmatic hydrothermal systems in China and its environmental
596 transport. *Science of The Total Environment*, 657, 1523-1534.
- 597 Hartl, H., Palm, R., & Fuchs, J. (1993). Ein neuer Parawolfram-Typ. *Angewandte Chemie*, 105(10), 1545-1547.
- 598 Hastings, J. J., & Howarth, O. W. (1992). A 183W, 1H and 17O nuclear magnetic resonance study of aqueous
599 isopolytungstates. *Journal of the Chemical Society, Dalton Transactions*, (2), 209-215.
- 600 Häufe, P. (1982). Raman-spectrophotometric determination of the tungstate anion and its isopolyanions in aqueous
601 systems. *Fresenius' Zeitschrift für analytische Chemie*, 310(5), 388-391.
- 602 Heinrich, C. A. (1990). The chemistry of hydrothermal tin (-tungsten) ore deposition. *Economic Geology*, 85(3), 457-
603 481.
- 604 Higgins, N. C. (1980). Fluid inclusion evidence for the transport of tungsten by carbonate complexes in hydrothermal
605 solutions. *Canadian Journal of Earth Sciences*, 17(7), 823-830.
- 606 Himeno, S., Yoshihara, M., & Maekawa, M. (2000). Formation of voltammetrically-active isopolyoxotungstate
607 complexes in aqueous CH₃CN media. *Inorganica Chimica Acta*, 298(2), 165-171.
- 608 Himeno, S., & Kitazumi, I. (2003). Capillary electrophoretic study on the formation and transformation of
609 isopolyoxotungstates in aqueous and aqueous-CH₃CN media. *Inorganica chimica acta*, 355, 81-86.
- 610 Hulsbosch, N., Boiron, M. C., Dewaele, S., & Muchez, P. (2016). Fluid fractionation of tungsten during granite–pegmatite
611 differentiation and the metal source of peribatholithic W quartz veins: Evidence from the Karagwe-Ankole Belt
612 (Rwanda). *Geochimica et Cosmochimica Acta*, 175, 299-318.

- 613 Jander, G., Mojert, D., & Aden, T. (1929). Über amphotere Oxyhydrate, deren wäßrige Lösungen und kristallisierende
614 Verbindungen. VIII. Mitteilung. Über Wolframate, Isopoly-und Heteropoly-Wolframsäuren. *Zeitschrift für*
615 *anorganische und allgemeine Chemie*, 180(1), 129-149.
- 616 Kokh, M. A., Akinfiev, N. N., Pokrovski, G. S., Salvi, S., & Guillaume, D. (2017). The role of carbon dioxide in the
617 transport and fractionation of metals by geological fluids. *Geochimica et Cosmochimica Acta*, 197, 433-466.
- 618 Klemme, S., Feldhaus, M., Potapkin, V., Wilke, M., Borchert, M., Louvel, M., ... & Testemale, D. (2021). A hydrothermal
619 apparatus for x-ray absorption spectroscopy of hydrothermal fluids at DESY. *Review of Scientific*
620 *Instruments*, 92(6), 063903.
- 621 Korges, M., Weis, P., Lüders, V. & Laurent, O. (2018). Depressurization and boiling of a single magmatic fluid as a
622 mechanism for tin-tungsten deposit formation. *Geology*, 46(1), pp.75-78.
- 623 Liu, Z., Mao, X., Deng, H., Li, B., Zhang, S., Lai, J., ... & Shang, Q. (2018). Hydrothermal processes at the Axi epithermal
624 Au deposit, western Tianshan: insights from geochemical effects of alteration, mineralization and trace elements
625 in pyrite. *Ore Geology Reviews*, 102, 368-385.
- 626 Liu, X., & Xiao, C. (2020). Wolframite solubility and precipitation in hydrothermal fluids: insight from thermodynamic
627 modeling. *Ore Geology Reviews*, 117, 103289.
- 628 Maksimovskaya, R. I., & Burtseva, K. G. (1985). 17O and 183W NMR studies of the paratungstate anions in aqueous
629 solutions. *Polyhedron*, 4(9), 1559-1562.
- 630 Mei, J., & Bao, Z. (2014). Side chain engineering in solution-processable conjugated polymers. *Chemistry of*
631 *Materials*, 26(1), 604-615.
- 632 Naumov, V. B., Dorofeev, V. A., & Mironova, O. F. (2011). Physicochemical parameters of the formation of
633 hydrothermal deposits: a fluid inclusion study. I. Tin and tungsten deposits. *Geochemistry International*, 49(10),
634 1002-1021.
- 635 Ng, K. Y. S., & Gulari, E. (1984). Spectroscopic and scattering investigation of isopoly-molybdate and tungstate
636 solutions. *Polyhedron*, 3(8), 1001-1011.
- 637 Ni, P., Wang, X. D., Wang, G. G., Huang, J. B., Pan, J. Y., & Wang, T. G. (2015). An infrared microthermometric study
638 of fluid inclusions in coexisting quartz and wolframite from Late Mesozoic tungsten deposits in the Gannan
639 metallogenic belt, South China. *Ore Geology Reviews*, 65, 1062-1077.
- 640 Pope, M. T. (1983). Heteropoly and isopoly oxometalates. *Springer-Verlag*.
- 641 Redkin, A. F., & Bondarenko, G. V. (2010). Raman spectra of tungsten-bearing solutions. *Journal of solution*
642 *chemistry*, 39(10), 1549-1561.
- 643 Redkin A. F., & Cygan G. L. (2020). Experimental Determination of Ferberite Solubility in the KCl–HCl–H₂O System
644 at 400–500 °C and 20–100 MPa. In: Litvin Y., Safonov O. (eds) *Advances in Experimental and Genetic*
645 *Mineralogy*. Springer Mineralogy. Springer, Cham. https://doi.org/10.1007/978-3-030-42859-4_7
- 646 Rios, F. J., Villas, R. N., & Fuzikawa, K. (2003). Fluid evolution in the Pedra Preta wolframite ore deposit,
647 Paleoproterozoic Musa granite, eastern Amazon craton, Brazil. *Journal of South American Earth Sciences*, 15(7),
648 787-802.
- 649 Ross-Medgaarden, E. I., & Wachs, I. E. (2007). Structural determination of bulk and surface tungsten oxides with UV–
650 vis diffuse reflectance spectroscopy and raman spectroscopy. *The Journal of Physical Chemistry C*, 111(41),
651 15089-15099.
- 652 Shvarov, Y. V. (2008). HCh: New potentialities for the thermodynamic simulation of geochemical systems offered by
653 Windows. *Geochemistry International*, 46, 834-839.

- 654 Truche, L., Bazarkina, E. F., Barré, G., Thomassot, E., Berger, G., Dubessy, J., & Robert, P. (2014). The role of S⁻³ ion
655 in thermochemical sulphate reduction: Geological and geochemical implications. *Earth and Planetary Science*
656 *Letters*, 396, 190-200.
- 657 Viggasina, M. F., Orlov, R. Y., Dadze, T. P., & Kashirtseva, G. A. (2000). Determination of thermodynamic parameters
658 of water-dissolved complexes at T < 360°C with the help of Raman spectroscopy: methods and equipment.
659 In *Raman Scattering* (Vol. 4069, pp. 103-108). International Society for Optics and Photonics.
- 660 Wang, X. S., Timofeev, A., Williams-Jones, A. E., Shang, L. B., & Bi, X. W. (2019). An experimental study of the
661 solubility and speciation of tungsten in NaCl-bearing aqueous solutions at 250, 300, and 350° C. *Geochimica et*
662 *Cosmochimica Acta*.
- 663 Wang, X., Qiu, Y., Lu, J., Chou, I. M., Zhang, W., Li, G., & Zhong, R. (2020a). In situ Raman spectroscopic investigation
664 of the hydrothermal speciation of tungsten: Implications for the ore-forming process. *Chemical Geology*, 119299.
- 665 Wang, X., Qiu Y., Chou, I. M., Zhang, R., Li G., & Zhong, R. (2020b). Effects of pH and Salinity on the Hydrothermal
666 Transport of Tungsten: Insights from In Situ Raman Spectroscopic Characterization of K₂WO₄ – NaCl – HCl –
667 CO₂ Solutions at Temperatures up to 400°C. *Geofluids*.
668 ID 2978984, 12 pages, 2020. <https://doi.org/10.1155/2020/2978984>
- 669 Weiner, H., Lunk, H. J., Friese, R., & Hartl, H. (2005). Synthesis, Crystal Structure, and Solution Stability of Keggin-
670 Type Heteropolytungstates (NH₄)₆NiII₀.₅ [α-FeIII_{0.4}W₁₁O₃₀NiII_{0.5}(OH₂)][⊖] n H₂O, (NH₄)₇Zn_{0.5} [α-
671 Zn_{0.4}W₁₁O₃₀Zn_{0.5}(OH₂)][⊖] n H₂O, and (NH₄)₇NiII_{0.5} [α-Zn_{0.4}W₁₁O₃₀NiII_{0.5}(OH₂)][⊖] n H₂O (n ≈
672 18). *Inorganic chemistry*, 44(22), 7751-7761.
- 673 Wesolowski, D., Drummond, S. E., Mesmer, R. E., & Ohmoto, H. (1984). Hydrolysis equilibria of tungsten (VI) in
674 aqueous sodium chloride solutions to 300. degree. C. *Inorganic Chemistry*, 23(8), 1120-1132.
- 675 Wood, S. A., & Vlassopoulos, D. (1989). Experimental determination of the hydrothermal solubility and speciation of
676 tungsten at 500° C and 1 kbar, 2. *Geochimica et Cosmochimica Acta*, 53(2), 303-312.
- 677 Wood, S. A. (1992). Experimental determination of the solubility of WO₃ (s) and the thermodynamic properties of
678 H₂WO₄ (aq) in the range 300–600 C at 1 kbar: calculation of scheelite solubility. *Geochimica et Cosmochimica*
679 *Acta*, 56(5), 1827-1836.
- 680 Wood, S. A., & Samson, I. M. (2000). The hydrothermal geochemistry of tungsten in granitoid environments: I. Relative
681 solubilities of ferberite and scheelite as a function of T, P, pH, and m NaCl. *Economic Geology*, 95(1), 143-182.
- 682 Zhang, Y., Yang, J. H., Chen, J. Y., Wang, H., & Xiang, Y. X. (2017). Petrogenesis of Jurassic tungsten-bearing
683 granites in the Nanling Range, South China: Evidence from whole-rock geochemistry and zircon U–Pb and Hf–
684 O isotopes. *Lithos*, 278, 166-180.

685 **Figure Captions**

686 **Fig.1:** Raman spectra of dissolved W-species in hydrothermal solution #5 (0.1 m W from $\text{Na}_6\text{W}_{12}\text{O}_{39}$, H_2O + 0.1 m NaCl, $\text{pH}_{25^\circ\text{C}}=5.60$) as a function of
 687 temperature.

689 **Fig.2:** (A) Raman spectra between 850 cm^{-1} and 980 cm^{-1} of solution #10 (0.1 m W from $\text{Na}_2\text{WO}_4 \cdot 2\text{H}_2\text{O}$ + 0.1 m NaOH) from 25°C , up to 400°C
 690 showing the band of tungstate ion B (WO_4^{2-}). (B) Raman spectra showing the band of tungstate ion (WO_4^{2-}) (species B) at 200°C and for different total
 691 tungsten concentrations: 0.01 m, 0.05 m, 0.1 m, 0.2 m. The intensity of (WO_4^{2-}) Raman band increases with W-concentration. (C) Linear correlation
 692 between the “B” species (WO_4^{2-}) Raman band area normalized to the water bending band area and tungsten volumetric concentration for different
 693 temperatures from 25 to 400°C . The line slope stands for the calibration coefficient K_T (in $\text{mol}\cdot\text{L}^{-1}$) at a given temperature for (WO_4^{2-}) ion. (D)
 694 Relationship between the calibration coefficient K_T of (WO_4^{2-}) ion and temperature.

696 **Fig. 3:** Raman spectra of four different W-bearing aqueous solution at four different pH conditions and at temperature ranging from 25 to 400°C . (A)
 697 Hyper-alkaline condition (solution #10, 0.1m total W concentration from $\text{Na}_2\text{WO}_4 \cdot 2\text{H}_2\text{O}$ + 0.1m NaOH, $\text{pH} = 13.02$ at 25°C) characterized by the
 698 dissolution of only one isolated species. (B) Circumneutral condition (solution #2, 0.1 m total W concentration from $\text{Na}_2\text{WO}_4 \cdot 2\text{H}_2\text{O}$ + 0.1 m HCl. pH
 699 = 6.87 at 25°C . (C) Slightly acidic condition (solution #5, 0.1 m total W concentration from $\text{Na}_6\text{W}_{12}\text{O}_{39} \cdot \text{H}_2\text{O}$ + 0.1 m NaCl, $\text{pH} = 5.60$ at 25°C). (D)
 700 Strongly acidic condition (solution #1, 0.1 m total W concentration from $\text{Na}_6\text{W}_{12}\text{O}_{39} \cdot \text{H}_2\text{O}$ + 0.1 m HCl, $\text{pH} = 1.10$ at 25°C). (E) Microscopic image of
 701 FSCC containing 0.1 m total W concentration from $\text{Na}_6\text{W}_{12}\text{O}_{39} \cdot \text{H}_2\text{O}$ + 0.1 m NaCl at $T=300^\circ\text{C}$, showing the precipitation of W-bearing solid phases.

703 **Fig. 4:** Raman spectra for the solution #R1 (0.1 m total W concentration from $\text{Na}_2\text{WO}_4 \cdot 2\text{H}_2\text{O}$ + 0.5 m CH_3COOH ; $\text{pH}_{T=25^\circ\text{C}}=4.00$). (A) W-speciation
 704 for fresh solution at $T = 25^\circ\text{C}$ (blue), immediately after heating at 200°C (purple), 300°C (orange) and 400°C (red), and at $T = 25^\circ\text{C}$ immediately
 705 after cooling (light blue) and two months after cooling (fuchsia). The blue spectrum in the upper part represents the W-speciation of the unheated
 706 solution after six months at 25°C . (B) Shows Raman spectra collected at various T on the same solution but after a pre-heating at 350°C for two days.

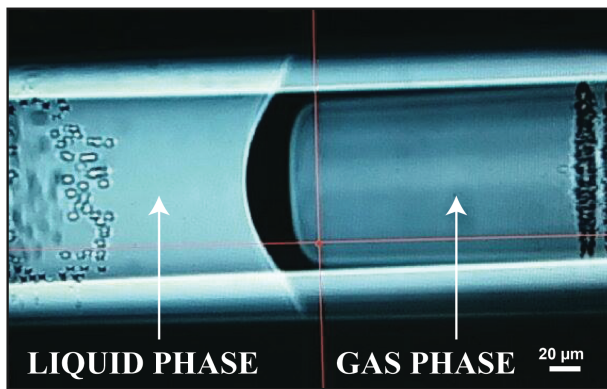
708 **Fig. 5:** Raman spectra showing the effect of W concentration (0.01 and 0.1 m total W concentration) on W speciation at temperature ranging from 25
 709 to 400°C and pH buffered by 0.5 m acetic acid ($\text{pH} \sim 4$ at 25°C). (A) Solution #18: 0.01 m total W concentration from $\text{Na}_2\text{WO}_4 \cdot 2\text{H}_2\text{O}$ + 0.5 m
 710 CH_3COOH , $\text{pH}_{25^\circ\text{C}} = 3.57$. (B) Solution #R1: 0.10 m total W concentration from $\text{Na}_2\text{WO}_4 \cdot 2\text{H}_2\text{O}$ + 0.5 m CH_3COOH $\text{pH}_{25^\circ\text{C}} = 4.00$. Tungsten speciation
 711 is unchanged whatever the temperature within this W concentration range.

713 **Fig. 6:** Raman spectra of W-bearing aqueous solutions in carbonate-bearing systems at 3 contrasted pH conditions and at temperatures ranging from 25
 714 to 400°C . (A) Circum-neutral condition (solution #12, 0.1 m total W concentration from $\text{Na}_2\text{WO}_4 \cdot 2\text{H}_2\text{O}$ + 0.14 m CO_2 , calculated $\text{pH} = 7.2$ at 25°C).
 715 (B) Alkaline condition (solution #11, 0.1 m total W concentration from $\text{Na}_2\text{WO}_4 \cdot 2\text{H}_2\text{O}$ + 1.1m NaHCO_3 , $\text{pH} = 8.30$ at 25°C). (C) Hyper alkaline
 716 condition (solution #13, 0.1 m total W concentration from $\text{Na}_2\text{WO}_4 \cdot 2\text{H}_2\text{O}$ + 1.2 m Na_2CO_3 , $\text{pH} = 11.85$ at 25°C).

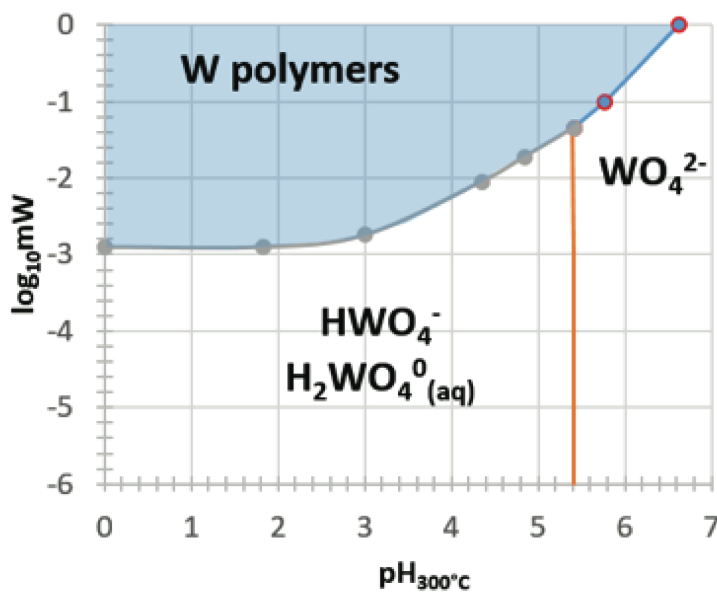
718 **Fig. 7:** Raman spectra of W-bearing aqueous solutions in chloride-bearing systems (NaCl) systems, from 25 to 400°C . In (A) acidic condition (solution
 719 #14, 0.1 m total W concentration from $\text{Na}_2\text{WO}_4 \cdot 2\text{H}_2\text{O}$ + 3.5 m NaCl + 0.5 m CH_3COOH , $\text{pH} = 5.28$ at 25°C). (B) Alkaline condition (solution #8, 0.1
 720 m total W concentration from $\text{Na}_2\text{WO}_4 \cdot 2\text{H}_2\text{O}$ + 3.6 NaCl, $\text{pH} = 9.56$ at 25°C).

722 **Fig. 8:** Tungsten speciation as a function of pH and temperature as deduced from a quantitative interpretation of the Raman spectra. (A) 25°C , (B)
 723 100°C , (C) 200°C , (D) 300°C . The total W concentration is 0.1 m.

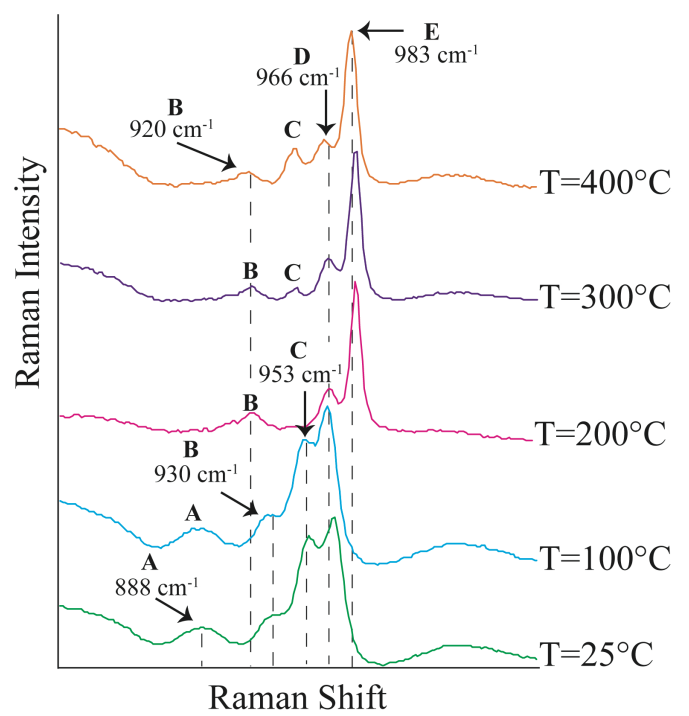
725 **Fig. 9:** Distribution in different W aqueous species at 300°C and P_{sat} as a function of pH at 0.1m total W concentration and 0.1m NaCl: (A) as determined
 726 from Raman spectroscopy data obtained in this study, and (B) considering the HWO_4^{2-} and H_2WO_4^0 from the literature. (C) The relative importance
 727 of W species in aqueous fluids with 1m NaCl and variable concentration of dissolved Na_2WO_4 as a function of pH and total W concentration under
 728 300°C and saturated vapour pressure. The lines correspond to the equality of mW in polymers and mW in other forms; the blue area indicates the
 729 conditions of W polymer predominance; the blue vertical dashed line indicates the neutral pH value at 300°C (5.70), the blue horizontal flesh indicates
 730 W concentration 1 ppm ($5.8 \cdot 10^{-6}$ mW). (D) The solubility of scheelite (CaWO_4) as a function of pH at 300°C in 5m NaCl aqueous solution and the
 731 concentrations of different species types. The stability of HWO_4^{2-} and H_2WO_4^0 in (B), (C), and (D) is taken according to Wang et al. (2019). The
 732 grey field indicated the pH when WO_3 can precipitate; the residual W concentration is below $5 \cdot 10^{-4}$ m.
 733
 734



Fused silica glass capillary

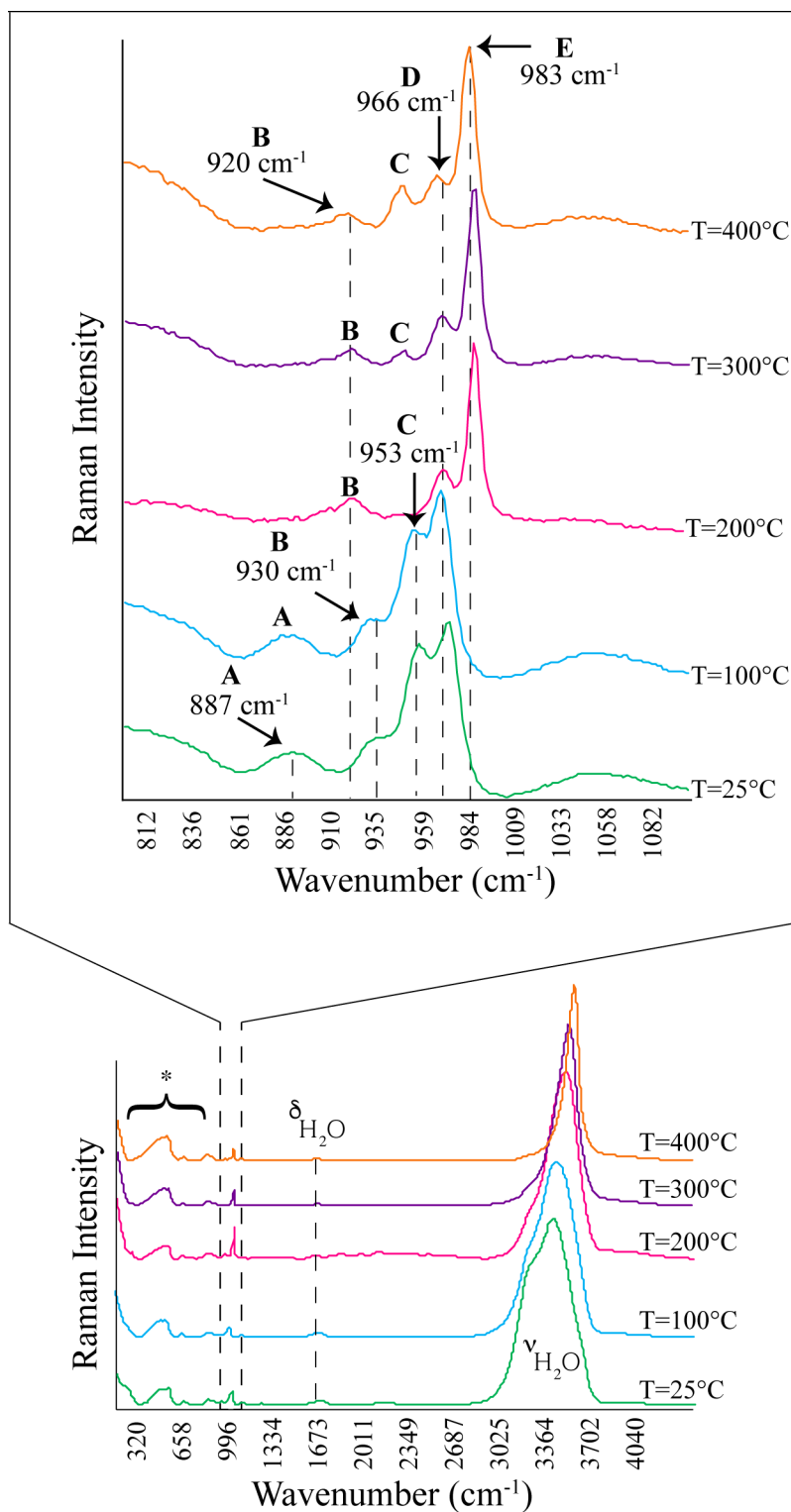


0.1 m W from $\text{Na}_6\text{W}_{12}\text{O}_{39}$, H_2O + 0.1 m NaCl, $\text{pH}_{25^\circ\text{C}}=5.60$



- A = asymmetric stretching (W=O) of C and D
- B = $(\text{WO}_4)^{2-}$: 930 cm^{-1}
- C = $(\text{W}_7\text{O}_{24})^{6-}$: 953 cm^{-1}
- D = $(\text{W}_{10}\text{O}_{32})^4$: 966 cm^{-1}
- E = $(\text{H}_2\text{W}_{12}\text{O}_{40})^6$: 983 cm^{-1}

Graphical Abstract



* Band of silica glass of the FSCC

Fig. 1

Sol. #10 : 0.1 m total W from $\text{Na}_2\text{WO}_4 \cdot 2\text{H}_2\text{O}$ +
 + 0.1 m NaOH

$\text{pH}_{T=25^\circ\text{C}} = 13$

Sol. #10.1 : 0.01 m total W from $\text{Na}_2\text{WO}_4 \cdot 2\text{H}_2\text{O}$ + 0.1 m NaOH

Sol. #10.2 : 0.05 m total W from $\text{Na}_2\text{WO}_4 \cdot 2\text{H}_2\text{O}$ + 0.1 m NaOH

Sol. #10.3 : 0.2 m total W from $\text{Na}_2\text{WO}_4 \cdot 2\text{H}_2\text{O}$ + 0.1 m NaOH

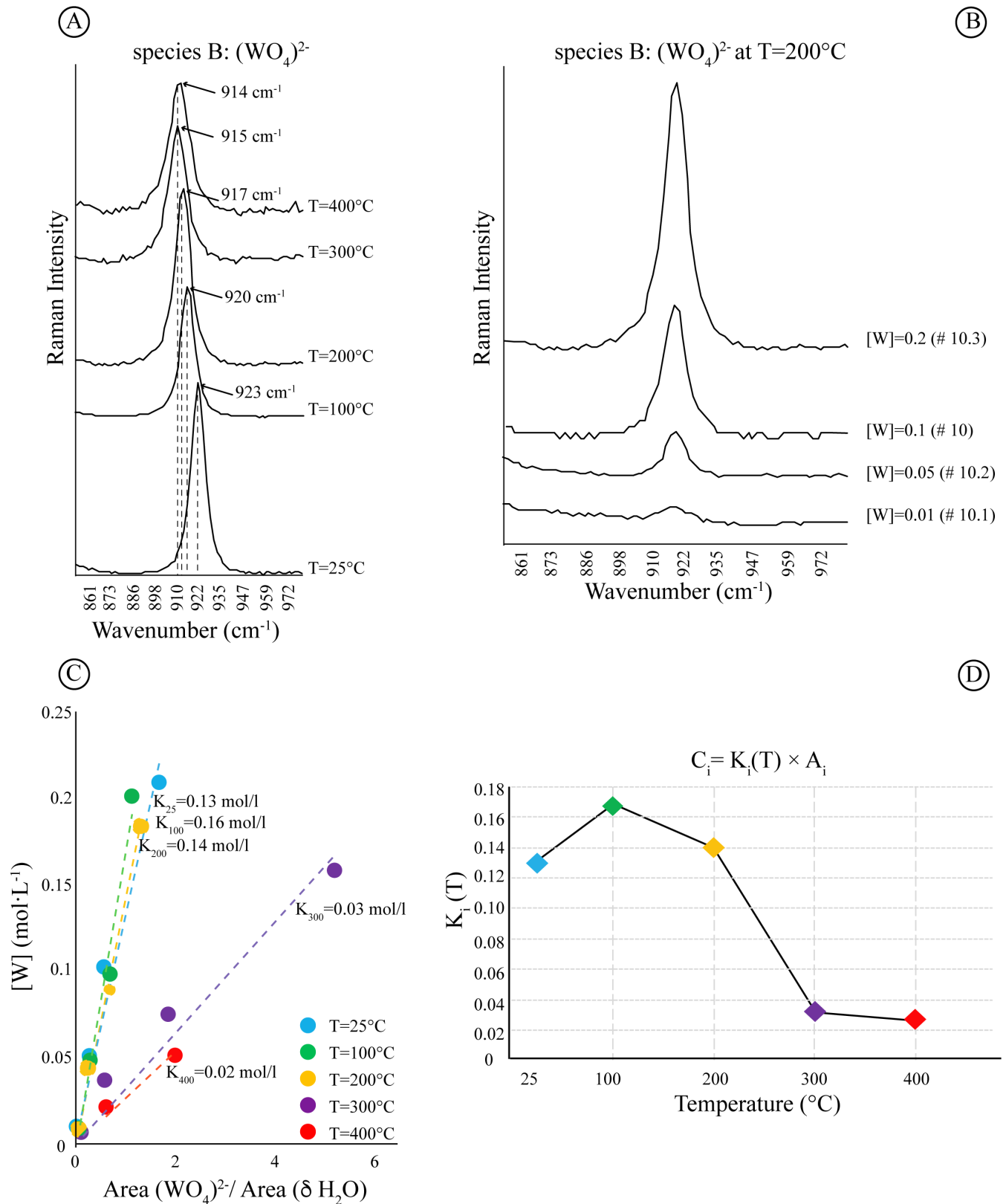


Fig. 2

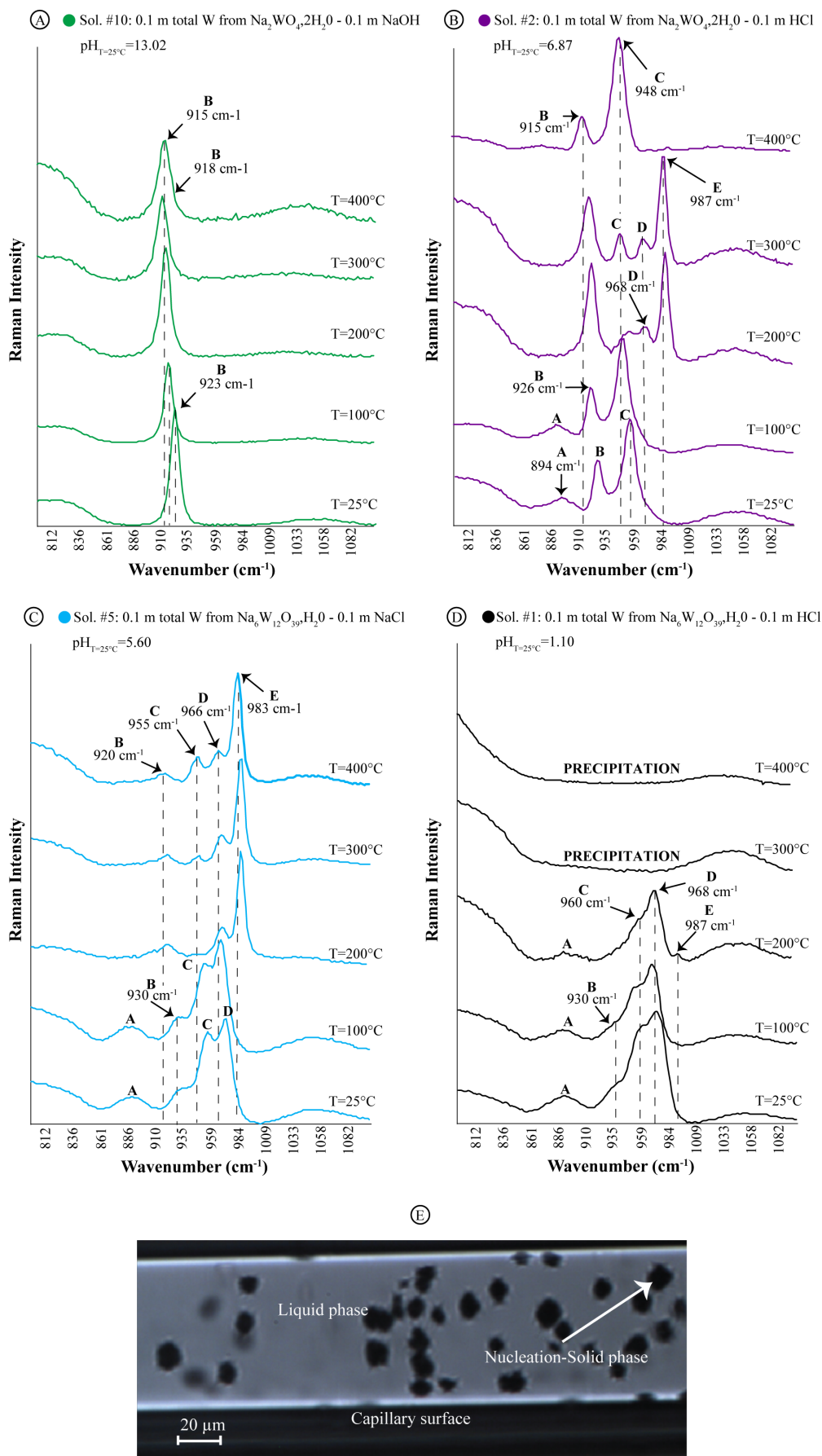


Fig. 3

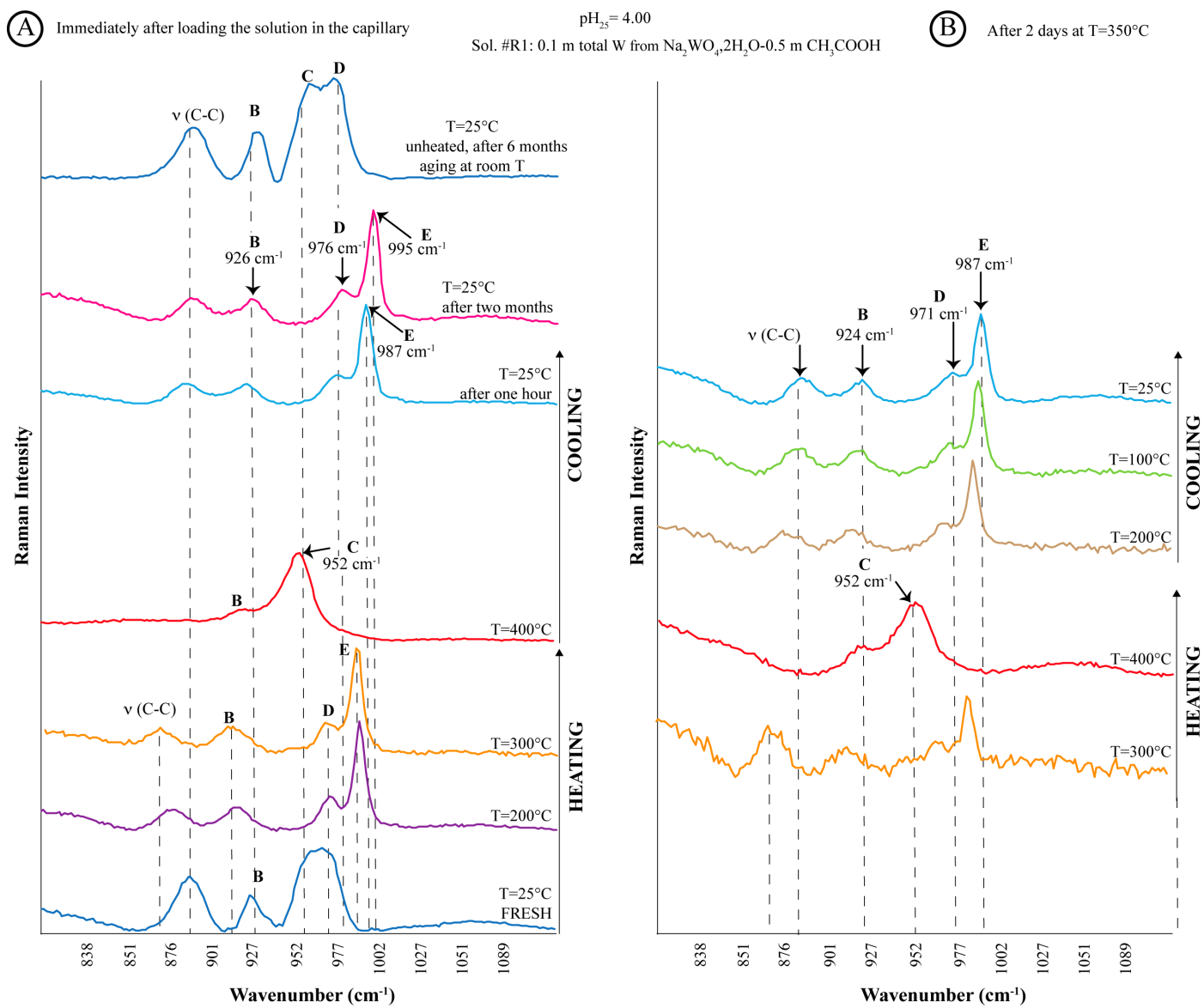
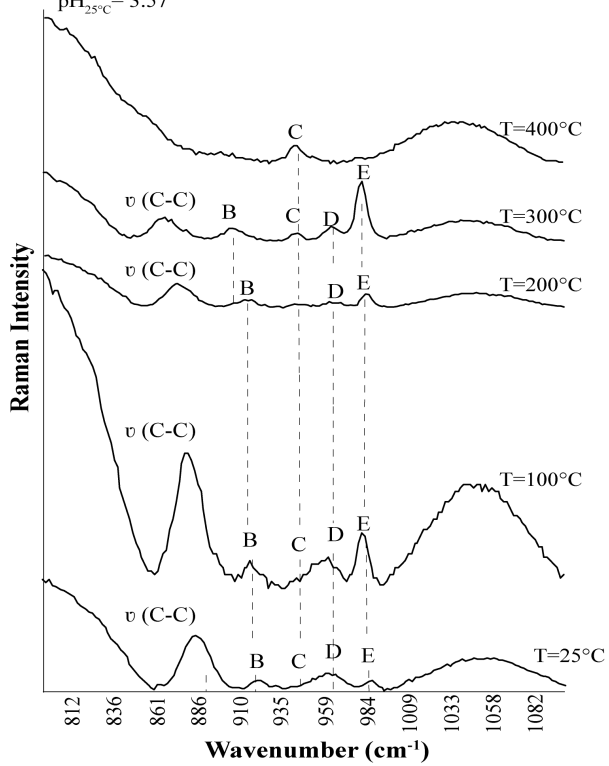


Fig. 4

Ⓐ ● Sol. #18: 0.01 m total W from $\text{Na}_2\text{WO}_4 \cdot 2\text{H}_2\text{O}$ - 0.5 m CH_3COOH
 $\text{pH}_{25^\circ\text{C}} = 3.57$



Ⓑ ● Sol. #R1: 0.1 m total W from $\text{Na}_2\text{WO}_4 \cdot 2\text{H}_2\text{O}$ - 0.5 m CH_3COOH
 $\text{pH}_{25^\circ\text{C}} = 4.00$

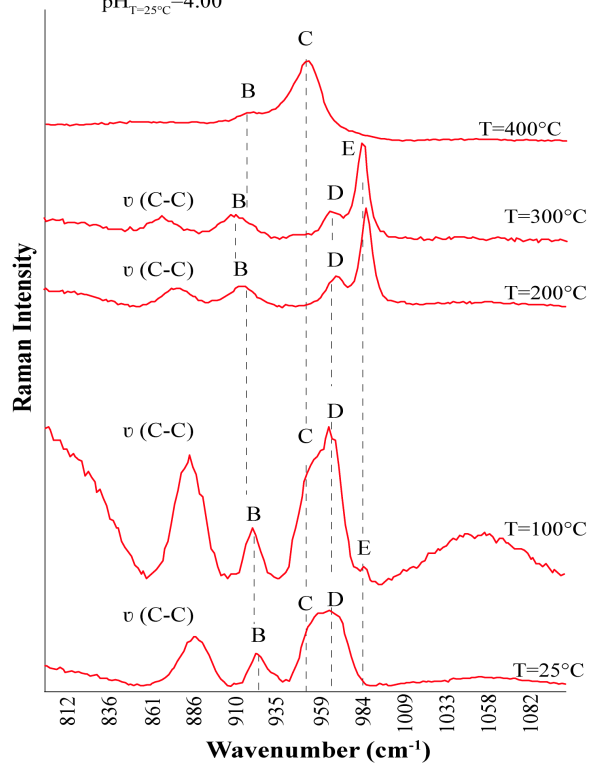


Fig. 5

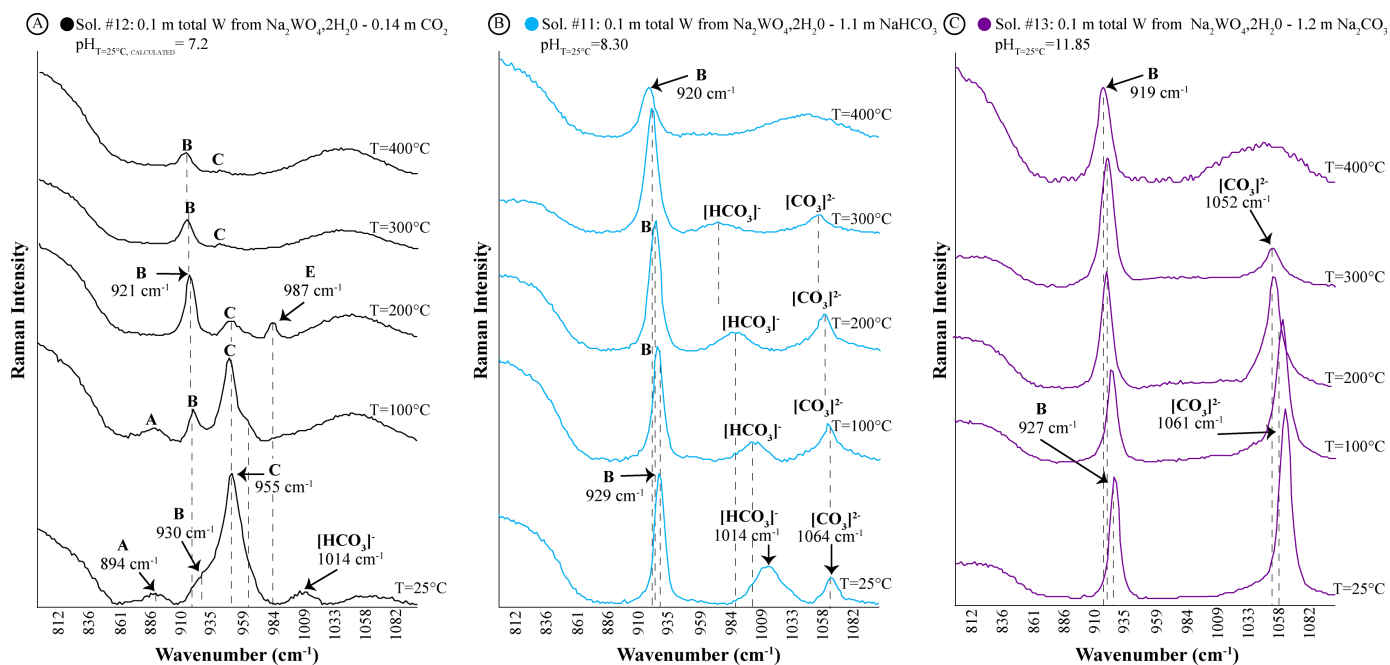


Fig. 6

(A) ● #14: 0.1 m total W from $\text{Na}_2\text{WO}_4 \cdot 2\text{H}_2\text{O}$ - 3.5 m NaCl - 0.5 m CH_3COOH (B) ● #8: 0.1 m total W from $\text{Na}_2\text{WO}_4 \cdot 2\text{H}_2\text{O}$ - 3.6 m NaCl

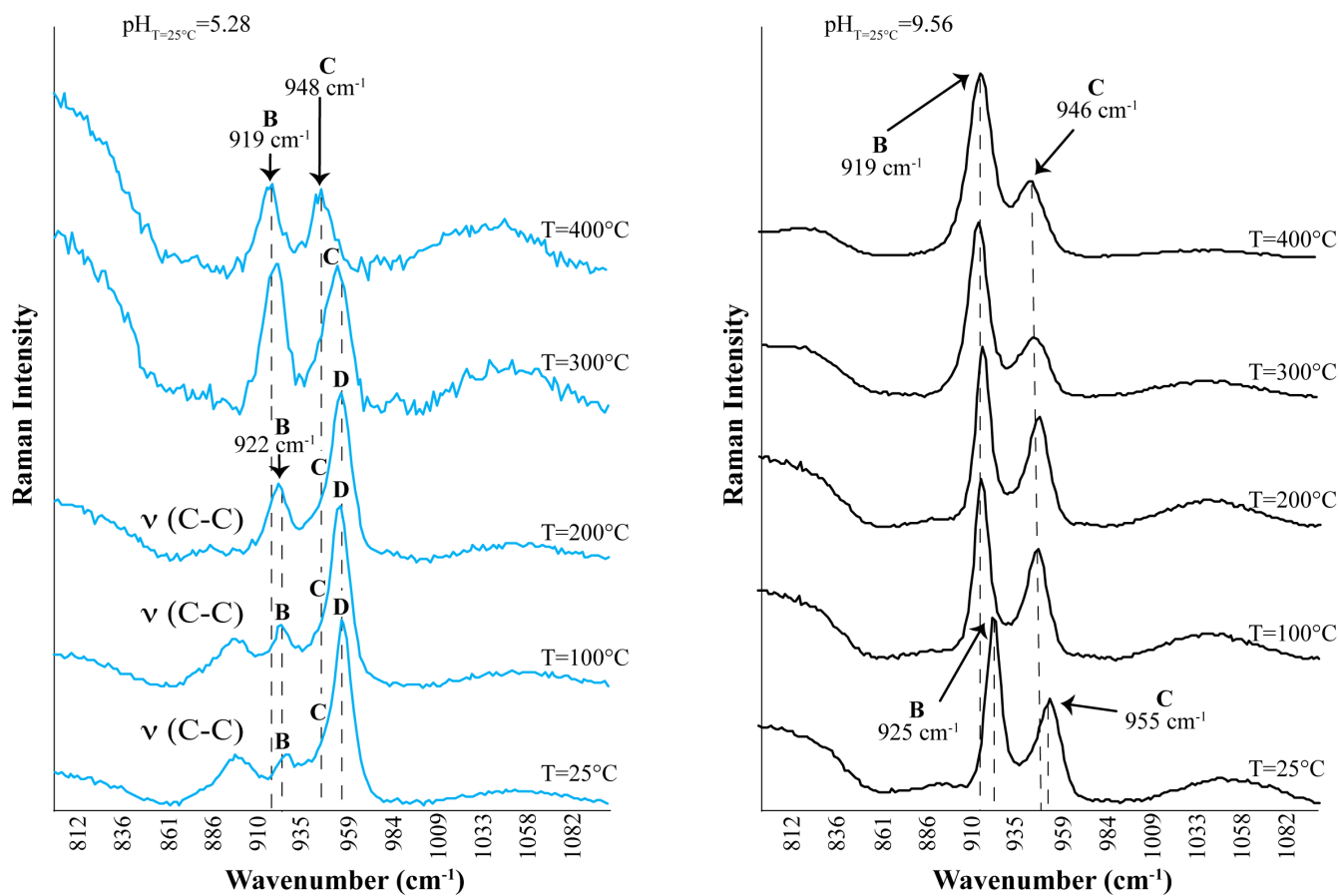


Fig. 7

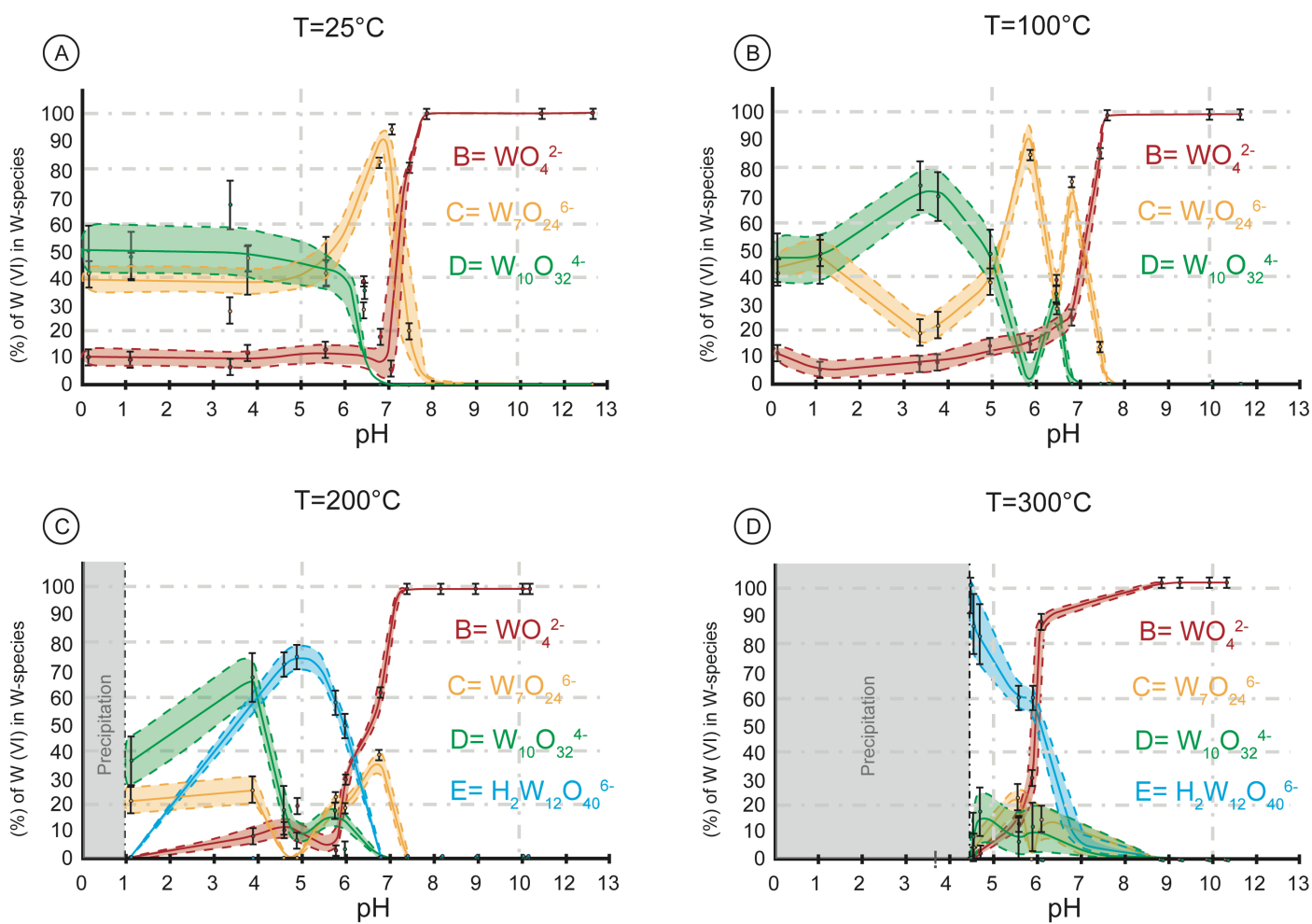


Fig. 8

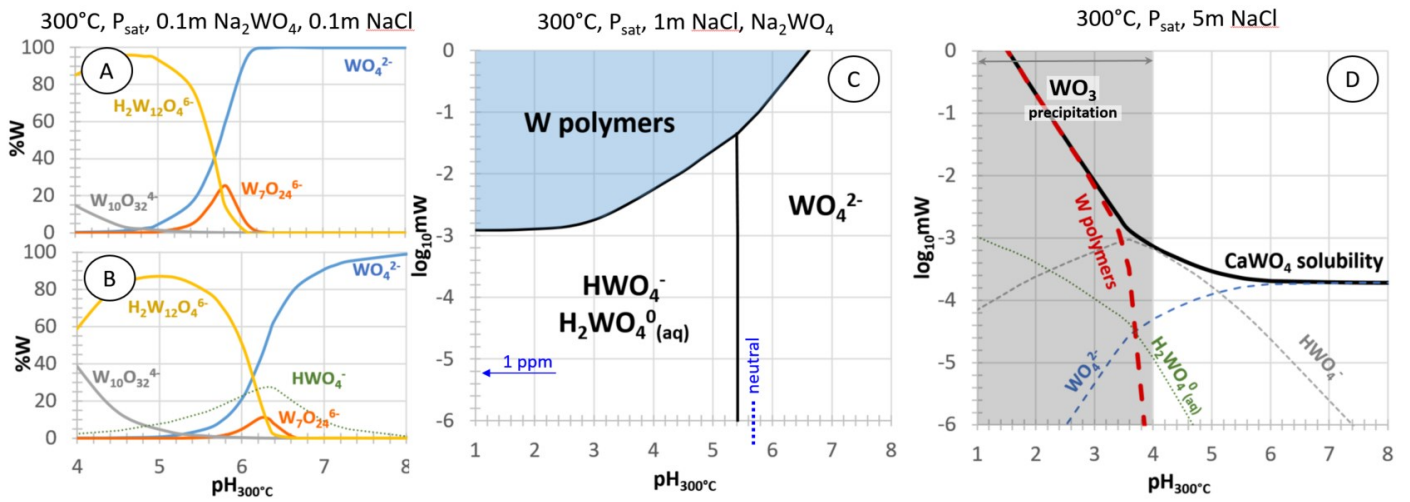


Fig. 9